# Plasmonic and Organic Nanostructures in Evanescent Optical Field


A thesis submitted towards partial fulfilment of
BS-MS Dual Degree Programme

by

P. Sruthi

under the guidance of

G.V. Pavan Kumar

Assistant Professor

Indian Institute of Science Education and Research
Pune

# Certificate

This is to certify that this thesis entitled "Plasmonic and Organic Nanostructures in Evanescent Optical Field" submitted towards the partial fulfillment of the BS-MS dual degree program at the Indian Institute of Science Education and Research Pune represents original research carried out by P. Sruthi at IISER, Pune, under the supervision of G.V. Pavan Kumar during the academic year 2012-2013.

Student
P. Sruthi

Supervisor
G.V. Pavan Kumar

# Acknowledgements

I am extremely grateful to Dr. G.V. Pavan Kumar for providing excellent laboratory facilities, constant support and advice regarding my work.

Words are not enough to express my thanks to my colleagues in the Photonics and Optical Nanoscopy Lab - especially Danveer Singh, Rohit Chikkaraddy, Partha Pratim Patra, Arindam Dasgupta. They provided invaluable help in troubleshooting experimental problems and synthesizing the nanostructures. The enlightening discussions I had with them helped me gain a deeper insight into basic concepts and expand my knowledge regarding current research. I also thank Arthur from Dr. Shouvik Datta's lab for always being there to help me with the thin film deposition; Venkatesh (Venki) and Madhan Gopal from the the Chemistry Department for helping us with glassware and chemicals during chemical synthesis.

Last but not the least, I would like to thank all my friends - Lokesh, Iti, Roshni, Bhargava, Anirban, Anees, Noaman, Swetha, Ramya, Himanshu, Harsha, Sachit, Srija, Kriti, Ravi, Abhijith for having been with me through highs and lows and for providing great motivation.

# Abstract

Nanostructures made from metals, inorganic semiconductos and organic molecules have interesting optical properties, which are very different from bulk material. These unique properties make them potential candidates for the development of miniaturized high speed photonic circuits and devices. They find applications in (i) optical waveguiding, (ii) nano bio sensing, (iii) lasing, (iv) polarized emission etc. Therefore, ongoing research is focused on learning the properties of these material nanostructures. The optical properties of these structures depend on various parameters, such as geometry, size, orientation, type of excitation, polarization of exciting light etc. Here we study the optical properties of metal and organic nanostructures under excitation using evanescent field created at a Total Internal Reflection (TIR) interface and how one can modulate these properties using such optical fields.

The work is broadly divided into two parts: (i) Plasmonic nanostructures, (ii) Organic micro/nano structures. In the first part, we experimentally show how polarization of evanescent optical fields can be used to modulate SERS intensity from a chemically-prepared, single silver-nanowire. By systematically varying the input polarization between p and s polarization we observed a modulation depth of 0.88 in SERS intensity. The scattered output light was polarized perpendicular to the nanowire axis with a modulation depth of 0.90. The SERS excitation of single nanowire in TIR geometry can be utilized as evanescent-mode nano-optical sensor. We also performed dark field microscopy studies on gold nanoparticles placed on a gold film. We observed that the gold NPs show a distinct donut shaped radiative mode, resulting from the vertical dipole moment induced in them by the gold film.

In the second part, we experimentally show how polarization of evanescent optical fields can be used to tune the photoluminescence (PL) signals from a single organic wire. By systematically varying the input polarization between p and s polarization we observed a shift of around 30nm in the PL spectra. Such a property can be utilized for obtaining tunable lasing from the wires.

# Contents

# Chapter 1

# Introduction

## 1.1 Why nanostructures?

In 1959, Richard Feynmann in his famous lecture "There's Plenty of Room at the Bottom" ([18]) said: "If we wanted to make a computer that had all these marvelous extra qualitative abilities, we would have to make it, perhaps, the size of the Pentagon. A practical difficulty is that the computer would be limited to a certain speed. Because of its large size, there is finite time required to get the information from one place to another. The information cannot go any faster than the speed of light - so, ultimately, when our computers get faster and faster and more and more elaborate, we will have to make them smaller and smaller. But there is plenty of room to make them smaller. There is nothing that I can see in the physical laws that says the computer elements cannot be made enormously smaller than they are now. In fact, there may be certain advantages."

And the advantages are many-fold. As the need for greater memory storage capacity, bandwidth, speed and miniaturization have been rising, the necessity to find technologies far better than the now widely used technology based on electronics is to be found. What poses a very attractive solution to these problems is photonic devices based on the localization, propagation, manipulation of photons by nanostructures, which form the interconnects and optical elements in the photonic circuits ([25], [11],). In the past few decades, it has been realized that nanostructures exhibit a variety of optical properties, due to their unique interaction with light, which is very different from their bulk counterparts. Some of the examples of such properties are: Bulk gold is yellow in color and mostly reflecting, but nanoparticles of gold exhibit a plethora of colors ranging from green to red depending on their size in the nano dimensions. Organic nanostructures show enhanced photoluminescence

efficiency in comparison to the individual molecules in a solution ([13]).

Ongoing research is focused both on understanding the fundamental aspects of why such unique optical properties are observed and on using these structures for building opto-electronic and photonic circuits. Probing the fundamental aspects have given us insight into many new physical phenomena such as localized surface plasmons, exciton coupling etc. From an application point of view, photonic nanostructures are used for designing and developing nano-optical elements in miniaturized high speed photonic circuits. Nanostructures have been made from many different materials: Metals, organic molecules, inorganic semiconductors, polymers ([49]). The many optical properties of Photonic structures that make them excellent candidates for developing photonic devices are given in the following paragraph.

**Light confinement beyond diffraction limit** gives rise to enhanced optical fields in nanoscale volumes ([48]), necessary for **sensing and detection** ([25]). One dimensional nano/micro structures act as **Optical Waveguides**, which can efficiently guide, manipulate, propagate and confine light within submicrometer volumes. Various groups have shown optical waveguiding properties in nanostructures made from metals ([14],[38],[23],[46]), inorganic semiconductors ([27],[7],[39]), organic molecules. Several studies have shown that plasmonic structures can be used for **Optical modulation**, such as for optical switching and gating ([40]). Nanoscale **lasers** have also been built using plasmonic, organic and inorganic nanostructures. Surface Plasmon lasers operate by amplification of plasmons, the greatly enhanced fields thus formed are ideal for building compact devices and circuits ([40]). Inspired by inorganic semiconductor lasers([43],[47]), recently lasers have been built even based on organic wires ([20]).

In view of the multitude of applications that are offered by nanostructures, it is essential to study their optical properties in great detail. The optical properties of these structures depend on various parameters, such as geometry, size, orientation, type of excitation, polarization of exciting light etc. Numerous studies have already been done on various kinds of nanostructures, of various geometries, typically under focused laser illumination through an objective lens. Here we study the optical properties of these nanostructures under excitation using evanescent field at a Total Internal Reflection interface and how one can modulate these properties using such optical fields. We separately consider plasmonic nanostructures and organic micro/nanowires in the presence of evanescent optical fields.

## 1.2 Plasmonic Nanostructures

The unique properties of metal nanostructures are rendered by surface plasmons - collective oscillations of electrons at a metal-dielectric interface, upon coupling to an incident electromagnetic field. The plasmons give rise to surface waves which decay exponentially into each of the two media - metal and dielectric, thereby confining the light to very small volumes. In addition, the wavelengths supported by the surface plasmons are different from that of a plane light wave. Therefore, the metal electrons increase the momentum of the light at the surface, allowing localization of electromagnetic fields beyond the diffration limit ([1])

An important question in nano-optics and -spectroscopy is how to control optical fields around plasmonic nanostructures, especially in the context of enhanced light-molecule interaction ([48]). A variety of nanoplasmonic geometries have been synthesized or fabricated ([19],[25],[26],[35]) and their field enhancement properties have been studied extensively ([5]). An important consequence of enhanced optical fields around a metallic nanostructure is the electromagnetic enhancement of surface enhanced Raman scattering (SERS), which plays a critical role in ultrasensitive detection of molecules ([34]). Although, large scale electromagnetic enhancement factors have been achieved with considerable success ([25]), the control of enhancement factor on a SERS substrate still remains a major challenge. This is because enhancement factors of SERS substrates are sensitive to various parameters such as size, shape, geometrical arrangement, chemical composition, local environment of the nanostructure etc. One possible way to tackle this constraint is to use individual plasmonic entities that can be used as a reliable SERS substrate.

Individual plasmonic nanowires made of silver or gold are promising candidates for SERS studies ([21],[16],[24]) because single-nanowire substrates can be optically manipulated and addressed with far-field optics ([44], [4]), and hence, their geometrical arrangement is relatively easy. Furthermore, they can be adapted for multiplexed nanophotonics application involving nano-optical waveguiding ([45]), SERS and optoelectronics ([15]). However, there is still an imperative need to develop experimental methods to control and modulate local optical fields around such isolated plasmonic nanowires without changing their geometrical parameters or optical alignment. Another relevant criterion is to develop experimental methods where the optical interrogation of the nanowire should not result in its physical deformation or chemical decomposition. This is specifically important in cases where the geometrical stability of nanowire depends on molecular capping agent surrounding its boundary ([41]).

One possible way to overcome the above-mentioned constraint is to excite plasmonic nanowire through total internal reflection (TIR). Advantage of performing SERS in TIR configuration is that excitation happens in dark-field mode thereby drastically improving the signal to noise ratio. TIR excitation is spatially confined to the interface, and hence it can be a powerful method to probe interfacial nanoscale structures and surfaces. More importantly, by varying the polarization of the input beam between these two polarized states, one would be able to observe change in the Raman scattering intensity from an isolated plasmonic nanowire. We resolve the polarization dependent Raman scattering from Ag NW, with respect to (i) input polarization of the evanescent field and (ii) orientation of the nanowire. By doing this, we construct SERS modulation matrix with respect to input and output polarization. Unlike conventional, point-illumination SERS microscopy, we use an evanescent optical field that excites the whole nanowire at an instant of time, and separately detect the SERS signal in orthogonal geometry using a high numerical objective lens. This dark-field method is a useful alternative to focused SERS excitation where focused laser beams can lead to photo-damage of chemically prepared nanostructure and/or the molecule adsorbed to it.

## 1.3 Organic micro/nano structures

Over the past decade, nanostructures based on organic molecules have emerged as a potential candidate for optical elements in modern photonic devices, mainly because of their diverse tunable properties, high photoluminescence efficiency, better waveguiding abilities, cost-efficient synthesis and good processability. The optical properties of organic nanostructures arise from the highly ordered $\pi$-stacked molecules.

Of the organic nanostructures, one dimensional waveguide structures have drawn great deal of interest due to their variety of optical properties such as polarized emission, lasing, enhanced emission, waveguiding. They can be easily adapted for multiplexed nanophotonics application involving nano-optical waveguiding, lasers, light-emitting diodes, transistors and optoelectronics ([15]).These crystalline nanostructures consist of luminescent molecules with low molecular weight and can be synthesized using simple and mild preparation methods. Most of the unique optical properties of these nanostructures are due to their high luminescence efficiency. One of the most attractive features of these organic molecules-based structures is their tunable optical properties, which have potential applications in building solid state miniature lasers.

Our study is focused on TIR based photoluminescence on an isolated sin-

gle organic microwire made up of a molecule called 1,5-diaminoanthraquinone, and show how the polarization of evanescent optical fields in total internal reflection configuration can be utilized to excite and modulate the photoluminescence wavelength from the wire in dark field. We show that the photoluminescence band shifts with respect to the input polarization of the evanescent field and show that this type of tunability of emission is not achievable using the conventional point-illumination PL microscopy or other PL spectroscopy techniques. An evanescent optical field excites the whole wire at an instant of time. Furthermore, TIR configuration facilitates excitation of the wire using certain polarization directions which are not possible using any other technique.

# Chapter 2

# Evanescent Fields

## 2.1 Total Internal Reflection and Formation of Evanescent fields

When light passes through a medium of high refractive index ($n_1$) into a medium of lower refractive index ($n_2$), it undergoes Total Internal Reflection at the interface between the two media if the angle of incidence of the light in the first medium with respect to the normal is greater than the critical angle. The critical angle is given by

$$\theta_c = sin^{-1}(n_2/n_1) \tag{2.1}$$

At the interface where light gets totally internally reflected, an electromagnetic field called the "Evanescent Wave" is created that decays exponentially into the second medium in the direction normal to the interface (z direction) and propagates along the surface (i.e., plane of incidence) ([6]).

## 2.2 Exponential Decay

The exponential decay of the evanescent electric field intensity is given as:

$$I_z = I_0 e^{-z/d} \tag{2.2}$$

where,

$$d = \frac{\lambda}{4\pi(n_1^2 sin^2\theta - n_2^2)^{-1/2}} \tag{2.3}$$

is known as the depth of penetration of the evanescent field. Here $\lambda$ is the wavelength of incident light and $\theta$ is the angle of incidence greater than the

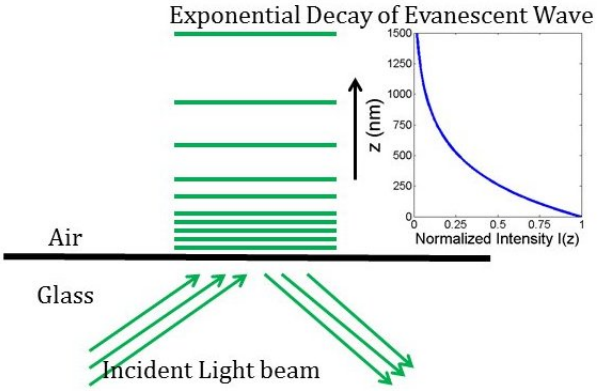


Figure 2.1: Illustration and plot showing the exponential decay of the evanescent field in the z direction. The graph is plotted using values of the parameters used in our studies ($\theta = 76.7°$, $n_1 = 1.519$, $n_2 = 1$, $\lambda = 532nm$)

critical angle and $n = n_2/n_1$. $I_0$ is the intensity at $z = 0$. For a glass-air interface, with $n_1 = 1.53$ and $n_2 = 1$ (which is what is the case for most of our studies), the exponential decay curve is shown in Figure 2.1. The normalized intensity plotted on the horizontal axis in the graph is with respect to the intensity at $z = 0$.

## 2.3 Intensity

The intensity at $z = 0$ in turn depends on the intensity of the incident beam of light ($\mathcal{I}$), polarization of incident light and the angle of incidence. If the polarization of incident light is parallel to the interface, with intensity ($\mathcal{I}_\parallel$), then the resultant evanescent intensity at $z = 0$ is given by

$$I_{0,\parallel} = \mathcal{I}_\parallel \left[ \frac{4cos^2\theta(2sin^2\theta - n^2)}{n^4cos^2\theta + sin^2\theta - n^2} \right] \tag{2.4}$$

Similarly, the intensity of evanescent field for perpendicular polarization of incident light is given by

$$I_{0,\perp} = \mathcal{I}_\perp . \left[ \frac{4cos^2\theta}{1 - n^2} \right] \tag{2.5}$$

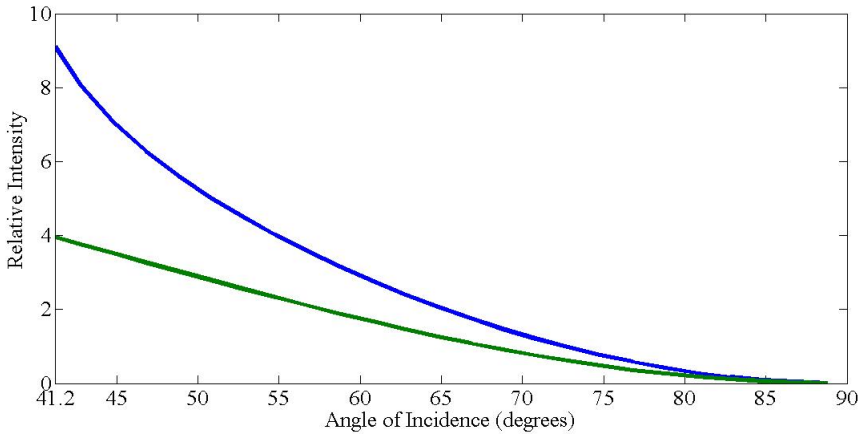


Figure 2.2: Intensity Profiles of Evanescent Field for p (blue) and s (green) polarized incident light at various angles of incidence starting from the critical angle (which is 41.2 degrees for the air-prism interface used in our studies). The intensity plotted on the y-axis is the ratio of the evanescent intensity at the interface to the intensity of incident light

## 2.4 Polarization

The electric field of the evanescent field ($E_x$, $E_y$ and $E_z$) depends on the amplitude of the incident light ($A_{\parallel,\perp}$) and incident phase factors ($\phi_{\parallel,\perp}$) at $z = 0$. Lets take a coordinate system where x-y plane is the interface and x-z is the plane of incidence (the plane containing incident ray of light and surface normal). Then, the electric field of the evanescent wave is given as:

$$E_x = \left[\frac{2cos\theta(sin^2\theta - n^2)^{1/2}}{(n^4cos^2\theta + sin^2\theta - n^2)^{1/2}}\right] A_{\parallel} e^{-i(\phi_{\parallel}+\pi/2)} \tag{2.6}$$

$$E_y = \left[\frac{2cos\theta}{(1 - n^2)^{1/2}}\right] A_{\perp} e^{-i\phi_{\perp}} \tag{2.7}$$

$$E_z = \left[\frac{2cos\theta sin\theta}{(n^4cos^2\theta + sin^2\theta - n^2)^{1/2}}\right] A_{\parallel} e^{-i\phi_{\parallel}} \tag{2.8}$$

where,

$$\phi_{\parallel} = tan^{-1}\left[\frac{(sin^2\theta - n^2)^{1/2}}{n^2cos\theta}\right] \tag{2.9}$$

and

$$\phi_{\perp} = tan^{-1}\left[\frac{(sin^2\theta - n^2)^{1/2}}{cos\theta}\right] \tag{2.10}$$

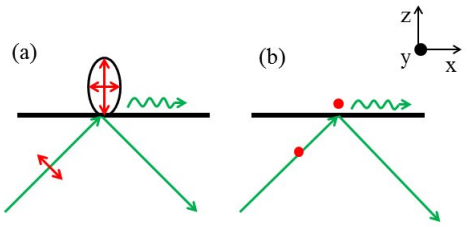


Figure 2.3: Electric field polarization (indicated in red color) for (a) p polarized incident light and (b) s polarized incident light (linearly polarized evanescent field created). Evanescent field propagation is in x direction.

From the above equations, it is very clear that if the incident light polarization is parallel to the plane of incidence (i.e., p polarized light), the evanescent electric field is elliptically polarized in the x and z directions, due to the fact that the two components are 90° out of phase with each other. In other words, the longitudinal non-zero component of the p polarized evanescent electric field makes it 'cartwheels' along the interface. Only for the perpendicular incident polarization (s polarized light), there exists a transverse electric field in the y direction. This is clearly illustrated in Figure 2.3.

Now, using equations (2.4) and (2.5), we plot the intensities of evanescent fields for the parallel and perpendicular incident polarizations, for various angles of incidence. For the glass-air interface, the critical angle is 41.2°. The intensity plotted on the y-axis in Figure 2.2 is the ratio of the evanescent intensity at the interface to the intensity of incident light. As one can see clearly, for most angles of incidence less than 90°, the intensity of p polarized evanescent field is greater than that of the s polarized evanescent field.

At $z = 0$, the components of magnetic field are given by

$$H_x = \left[\frac{2cos\theta(sin^2\theta - n^2)^{1/2}}{(1-n^2)^{1/2}}\right] A_\perp e^{-i(\phi_\perp - \pi)} \tag{2.11}$$

$$H_y = \left[\frac{2n^2 cos\theta}{(n^4 cos^2\theta + sin^2\theta - n^2)^{1/2}}\right] A_\parallel e^{-i(\phi_\parallel - \pi/2)} \tag{2.12}$$

$$H_z = \left[\frac{2cos\theta sin\theta}{(1-n^2)^{1/2}}\right] A_\perp e^{-i\phi_\perp} \tag{2.13}$$

## 2.5 Goos-Hänchen and Imbert-Federov Effect

On total internal reflection, a finite cross section *linearly polarized* light wave undergoes a lateral shift. This effect is called the Goos-Hänchen Effect ([9]).

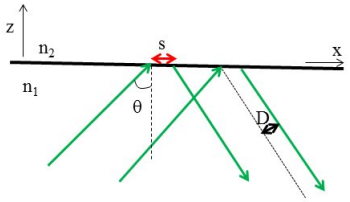


Figure 2.4: Goos-Hänchen Shift

In other words, a part of the energy of the incident beam crosses the interface, propagates parallel to it in the lower refractive index medium for a distance (s), before coming back into the first medium. See figure 4. The Goos-Hänchen Shift is then given by $D = s.cos\theta$. Without going into the details of its derivation, the dependence of the Goos-Häenchen Shift on incident light angle is given by the following equations:

For perpendicular incident electric field polarization:

$$D_{\perp} = \frac{\lambda}{\pi} \frac{sin\theta}{(sin^2\theta - n^2)^{1/2}} \tag{2.14}$$

And for incident electric field parallel to the plane of incidence, the Goos-Hänchen shift is given by

$$D_{\parallel} = \frac{n^2}{sin^2\theta(1+n^2) - n^2} D_{\perp} \tag{2.15}$$

Therefore, for large angles of incidence (close to 90°), the Goos-Hänchen Shift is of the order of just a fraction of a wavelength, whereas, it is infinity for angle of incidence equal to the critical angle (the angle of incidence where the angle of refraction becomes zero and light travels parallel to the interface after entering lower refractive index medium). This effect can be understood well from Figure 2.4. The transverse shift that *circularly polarized* or *elliptically polarized* optical beams undergo after total internal reflection is called Imbert-Federov effect ([36]).

## 2.6 Applications

An absorber or scatterer placed in the evanescent field gets excited and emits/scatters light. Thus, the near-field evanescent electromagnetic field is converted into far-field propagating wave. Since the evanescent field decays within a distance of few nanometers, only the scattered/emitted light

is seen. Hence, the background signal is completely eliminated and one uses evanescent fields to do dark-field (DF) microscopy and spectroscopy. Another application of this is extensively used in the field of biology - Total Internal Reflection Fluorescence. This technique uses the fluorescence from molecules present at the interface to study a wide range of biochemical and biophysical phenomena. If a layer of unmatched refractive index is present between Medium 1 and 2, Frustrated Total Internal Reflection occurs. This phenomenon also has found many applications in design of laser cavity ([12]), Analytical Laser Spectroscopy ([8]). Evanescent fields have been used for studing the phenomenon of optical trapping and array formation ([30],[29]). It has also been used for exciting surface plasmons on thin metal layers (Maeir), for performing dark feld spectroscopy on single metal nanoparticles ([17],[10]) and plasmonic trapping ([37]). What we are interested in our work is to see how the polarization of the evanescent field affects elastic and inelastic scattered light from many types of nanostructures, made up of metals and organic molecules.

If the entities (absorbers, scatterers) placed at the interface undergo magnetic dipole transitions, the evanescent magnetic field given also become important. In our studies however, this won't be very relevant.

# Chapter 3

# Instrumentation, Experimental Techniques and Chemical Synthesis Methods

## 3.1 Optical Set-up

The experimental set-up used is shown in the schematic diagram of Figure 3.1. Light from the laser enters the prism and undergoes total internal reflection at the interface. A lambda/2 waveplate in the path is used to change the direction of polarization of the light and a lens is used to focus the beam at the point of TIR. The cover slip containing the sample (nanostructures) was index matched with the prism. The sample is excited by the evanescent field. Light emitted from the sample is collected using a high numerical aperture objective lens. This light is diverted either towards a CCD camera to obtain optical or dark-field Rayleigh image or towards confocal Raman spectrometer after rejecting Rayleigh line. An analyzer placed in the path can be used to resolve the output polarization. In the next few paragraphs, each instrument/device/part used in the experiment will be explained.

**Laser** : Laser light source of 532nm (Ventus VIS 532) from Laser Quantum was used for excitation in all our studies. The power of the laser could be adjusted from 50mW to 1500mW. It emits light of horizontal polarization. Therefore, with respect to the plane of incidence of the prism, the light coming directly from the laser would be s polarized.

$\lambda/2$ **waveplate** : A waveplate is an optical device which is used to change the polarization of light that is passed through it. For linearly polarized light, a half waveplate has the effect of rotating the electric field direction by $2\theta_e$, where $\theta_e$ is the angle that the incident electric field makes with the fast axis of

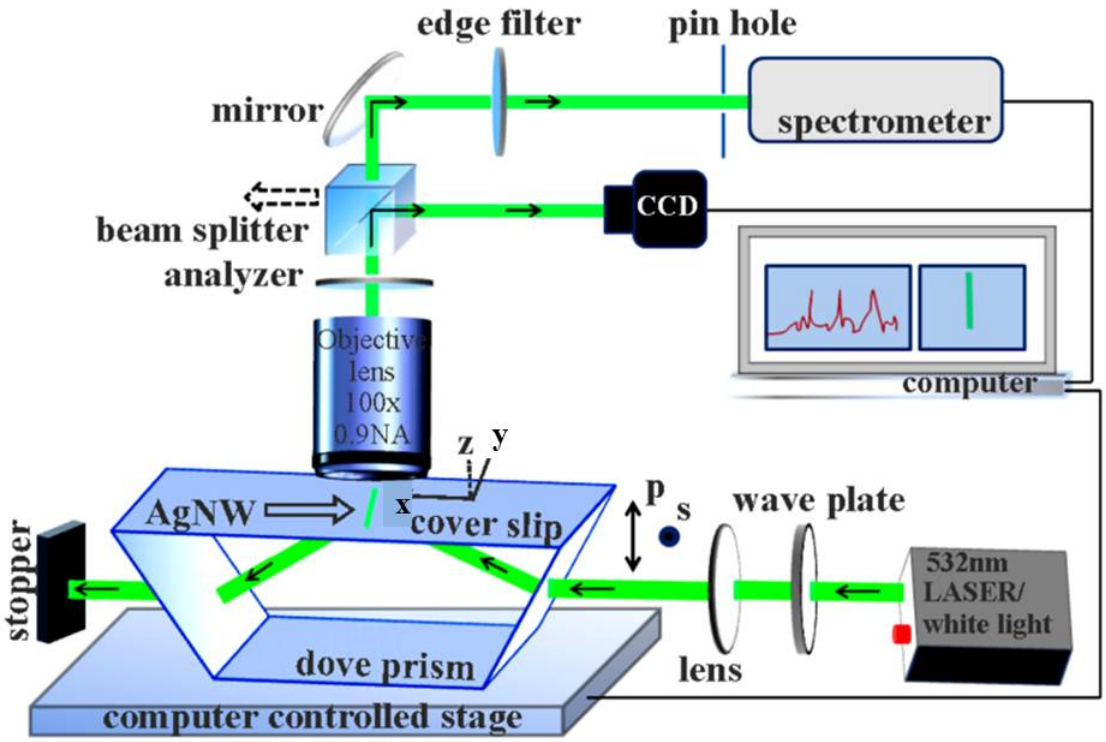


Figure 3.1: Schematic of the multi-function optical microscope used in this work. The microscope was used to capture dark-field white light spectra, monochromatic Rayleigh scattering image and surface enhanced Raman scattering signal from nanostructures (for example, AgNW here). Nanowire length was along y axis and the incident k vector was along x axis. The signal collection was along z-axis.

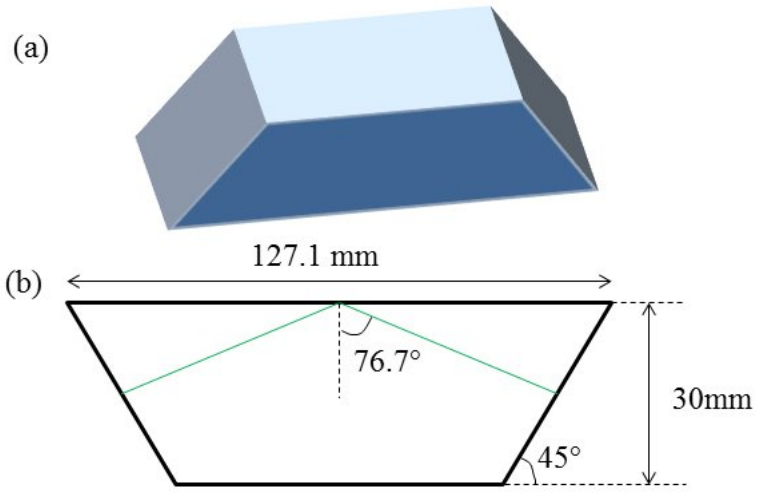


Figure 3.2: (a) The dove prism (b) Figure illustrating the dimensions of the prism

the waveplate. Waveplates used in our studies were products from Thorlabs.

**Dove Prism** : The Dove Prism used in our experiments is a product of Thorlabs - PS 993. The dimensions of the prism are given in the figure below. Using these dimensions and trigonometric relations, one can find the angle of incidence at the TIR interface as 76.7°. The prism is made up of glass called N-BK7. The refractive index of this at 532nm is 1.519, therefore yielding a critical angle of 41.2° for glass-air interface.

**Objective Lens** : We used a high numerical aperture ($NA = 0.9$) 100X objective lens from Olympus for collection. Numerical Aperture is given by $NA = nsin\mu$ where $\mu$ is half of the angular aperture (A) shown in figure and n is the refractive index of the medium from which light passes and is collected. If the NA is large, it means that more oblique rays can enter the objective lens.

**Imaging and Spectroscopy** : The light collected is sent either to a Charge Coupled Device (Synapse, Horiba Jobin Yvon) for forming image or to a spectrometer. For collecting the Raman spectrum, the light is first passed through an edge filter for 532nm light. Therefore, the Rayleigh scattered light (of 532nm) is eliminated. All Raman spectra, dark field spectra and photoluminescence spectra taken in our studies were recorded on high resolution confocal microscopy system - LabRam HR, Horbia Jobin Yvon, France.

**Lenses and Polarizers** : All lenses and polarizers used in this work are

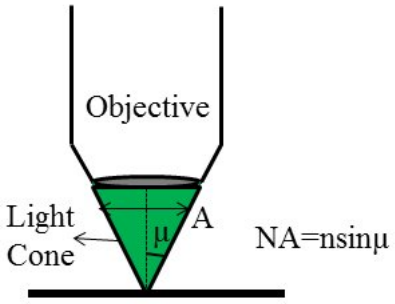


Figure 3.3: Simple illustration showing the angular aperture of an objective lens

products of Thorlabs. For focusing the light entering the prism, we used a plano convex lens of focal length . For white light TIR dark field imaging, first a f = 60mm plano convex lens is used to collimate the light from a 100W halogen lamp and a plano convex lens of focal length 125mm is used for focusing the light at the TIR spot.

## 3.2 Preparation of Nanostructures

### 3.2.1 Synthesis of Silver Nanowires

Silver nanowires were chemically prepared using the well-know polyol process ([41]). Solution A of 0.085M AgNO3 (Sigma Aldrich) in 3 ml of ethylene glycol(EG) (Sigma Aldrich) and Solution B of 0.34M (calculated by the monomerâĂŹs MW) poly(vinyl pyrrolidone) (PVP)(MW 55 000; Sigma Aldrich)in 3ml of EG are prepared at room temperature. Solutions A and B were mixed and 6ml of this solution was added drop wise during a 30 min time period to 5ml of EG taken in a round bottom flask preheated to 160° C in oil bath. After injection, the solution was heated at 160° C for 1 h. Finally, the whole solution was cooled and centrifuged at 2000 rpm for 10 min, twice with acetone and 10 times with water to remove EG and PVP. Final suspension was dispersed in water. This procedure yielded a variety of single crystalline Ag NW configurations of which pairs of Ag NWs were chosen for the current study. Figure shows transmission electron microscopy (FEI Tecnai F20, 200 kV) image of a part of an Ag nanowire. As is clear from the image, the diameter of the wires are around 100nm. The lengths (not shown here) are around 20$\mu$m, as seen using bright field images (shown

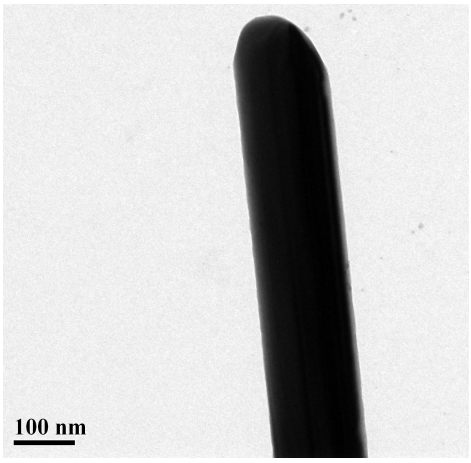


Figure 3.4: Transmission electron microscopy image of a section of an AgNW

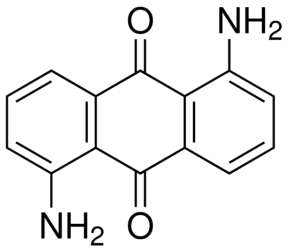


Figure 3.5: 1,5- di amino anthraquinone: The organic molecule that is used for preparation of organic wires

later in the next chapter).

### 3.2.2 Synthesis of Organic micro and nano- Wires

Organic nanowires of 1,5-diaminoanthraquinone (DAAQ) are synthesized using a physical vapour deposition technique developed by Zhao et.al. The structure of DAAQ is shown in the figure 3.5.

10mg of DAAQ in 20 ml of ethanol is heated at 60°C for 5-6 hours so as to form a thin, uniform coating of DAAQ on the inner wall of a round bottom flask. A small glass substrate (cover slip) is inserted through the mouth of the flask and left dangling in the middle (without touching the walls of the flask). The layer of DAAQ is now heated to $170 - 190$°C. The resultant vapors condense on the glass substrate, forming nuclei first. The process is illustrated in figure 3.6.

The figure 3.7 shows optical images of the wires thus formed. The length

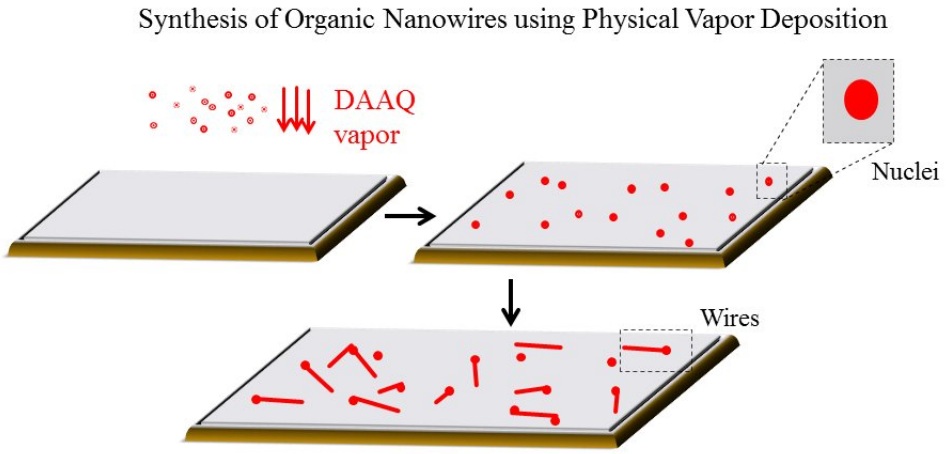


Figure 3.6: Simple representation of the process of physical vapor deposition for synthesis of Organic Wires made up of DAAQ molecules

and diameter of the wires can be controlled by the growth conditions (temperature to which the flask is heated during physical vapor deposition and the amount of time for which it is heated).

### 3.2.3 Synthesis of Silver Nanoparticles

Silver nanoparticles (Ag sols) were synthesized using the standard citrate reduction technique ([28]). The approximate size of each of these particles synthesized using this method is around 60nm.

### 3.2.4 Synthesis of Gold Nanoparticles

Gold nanoparticles (Au sols) also were also prepared using the standard process of citrate reduction ([28]). The approximate size of each of these particles synthesized using this method is around 30nm.

### 3.2.5 Sputtering Process for deposition of Metal thin film

The process in which atoms from a target material are ejected due to their bombardment by high energy particles is called sputtering. We used the sputter technique to produce thin films of gold on glass substrates (Q150T ES Turbo-Pumped Sputter Coater - a high resolution sputter and high vacuum

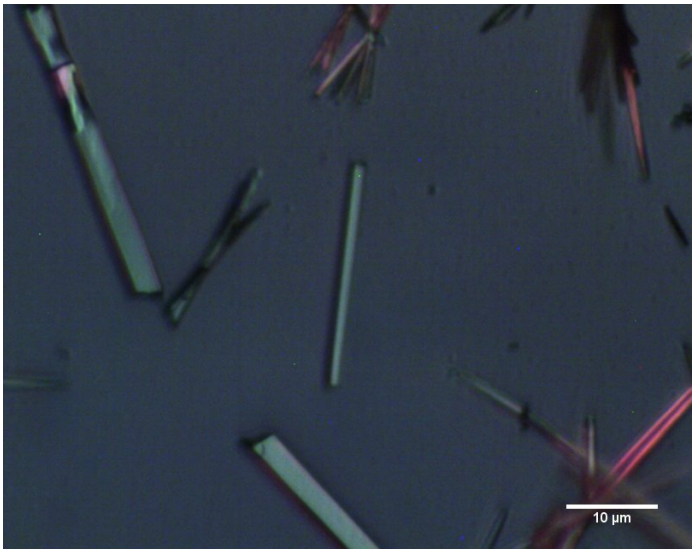


Figure 3.7: Optical bright field image of organic wires on a glass substrate

carbon coater). High energy Argon ions (positively charged) are created and made to bombard with gold target (placed at a negative potential). The gold atoms then deposit on the glass substrate. In our experiments, films of thickness 40nm were prepared.

# Chapter 4

# Optical properties of Plasmonic Nanostructures in evanescent field

In this chapter, we study the optical properties of metal nanowires and nanoparticles in an evanescent field, which is a result of their plasmonic nature. Metals can be considered as a sea of free electrons (plasma) moving against a fixed background of positively charged ions and for over a wide ranges of frequencies, the optical properties of metals can be described by this plasma model. Collective oscillations of these electrons at the interface of metal and dielectric are called surface plasmons.

In case of metal films and wires, the electromagnetic excitations that result due to the coupling of electromagnetic fields to oscillations of the electrons (Surface plasmon polaritons) propagate along the interface, but decay exponentially in the perpendicular direction into both the dielectric and the metal ([2]). Surface plasmon polaritons (SPP) cannot be excited by just illuminating light at a metal-dielectric interface. This is because the momentum (k) vector of SPP is higher than that of plane light wave. Therefore, a prism configuration (metal on top of a dielectric, excited using TIR evanescent field, for example) is used to excite surface plasmons. The reason for this is that, the k vector (and hence the momentum) of SPP is greater than that of plane light wave, at all frequencies below the plasma frequency (above which the metal loses its metallic character). A detailed derivation of the dispersion relation for SPPs can be found in the appendix.

Gold and silver are the most commonly used plasmonic substrates for the reason that the plasmonic properties of these metals can be seen at visible frequencies. Of the two, silver shows better plasmonic electric field enhancements and lesser losses. This is because, gold undergoes interband transitions at the green frequencies. This leads to absorption of light at the blue-green region of the electromagnetic spectrum, leading to greater losses

and lesser plasmonic character.

## 4.1 Experimental Results for Silver Nanowire

Figure 4.1(a) shows the optical image of a single silver nanowire. Figure 4.1(b) shows the dark-field Rayleigh image of single Ag NW excited by p-polarized light at 532nm excitation, and Figure 4.1(c) shows the corresponding image obtained by s-polarized light. Figure 4.1 (b) and (c) clearly shows a high contrast, wide-field Rayleigh image of a single Ag NW. Note that the Rayleigh scattering intensity reduces when we go from p- to s-polarized illumination. Whereas it is true that evanescent intensity for p-polarized evanescent field is greater than that for s-polarized field (as was seen from figure 2.2 in Chapter 2), it does not completely explain the drastic difference in the intensity. The main reason why we see this difference in intensity is because surface plasmons are excited in the silver nanowire when the incident light is p polarized, as explained later.

This especially becomes evident when we take the Surface enhanced Raman scattering spectrum from these wires. Raman scattering is an inelastic scattering phenomenon, where a molecule scatters an incident photon of frequency ($\nu_i$) at a different frequency of ($\nu_o$). If the molecule was originally in the ground state, then this occurs because the incident photon excites the molecule to a virtual state and the molecule on de-excitation returns not to the original ground state but to a higher vibrational level (Stoke's Shift). If the molecule was originally in an excited vibrational level, then additional energy is emitted on de-excitation to the ground level (Anti-Stoke's Shift). Typically Raman scattering cross sections are $10^6$ orders of magnitude smaller than fluorescence and depends linearly on the incident intensity ([32]). The Raman scattering signals are very difficult to detect (due to very small cross section $10^{-31} cm^2$/molecule and one needs very high intensities to be able to detect better signals. Surface enhanced Raman Scattering is a process where the Raman signals from a molecule are enhanced due to the molecule being present in the vicinity of localized fields of a rough metal surface or metal nanostructures. The enhancement is due to two reasons: (i) Chemical Enhancement: This is due to change in the chemical environment of the molecule. The enhancement factor in this case doesn't exceed a factor of 100. (ii) Electromagnetic Enhancement: This is due to the increased electromagnetic field intensities, as a result of excitation of surface plasmons in the metal.

Figure 4.1(d) shows the dark-field SERS spectra from single Ag NW with p-polarized illumination with accumulation time of 10 seconds. The inset in

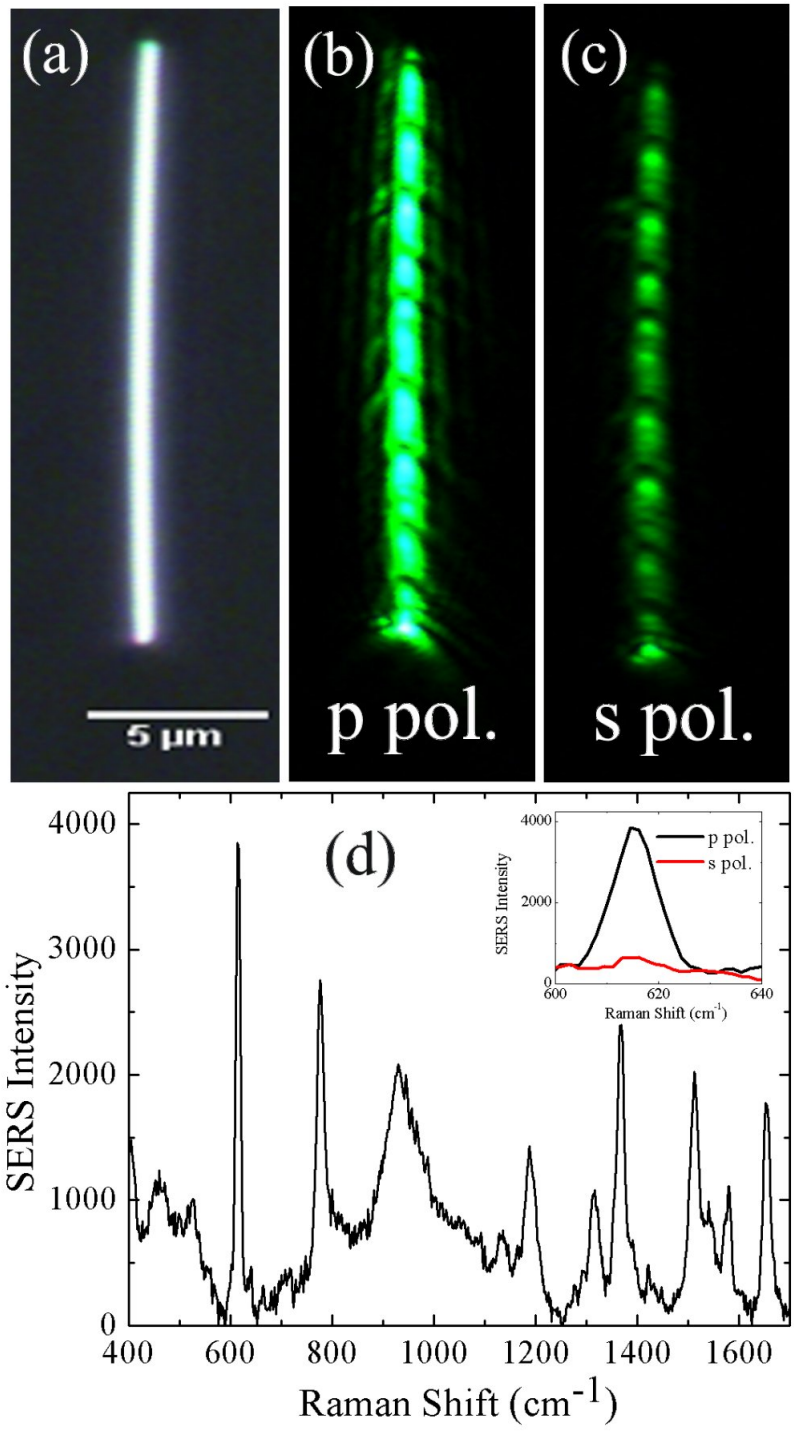


Figure 4.1: Single Ag nanowire (diameter = 300nm, length= 25 $\mu m$)- images and SERS spectra. (a) Optical image. Dark-field Rayleigh scattering image excited by (b) p-polarized light and (c) s-polarized light at 532nm. (d) Dark-field SERS spectra of rhodamine 6G from single Ag nanowire for p polarization illumination. The inset spectra compare $612cm^{-1}$ mode for p and s polarized excitation. The signal accumulation time was 10s for all the spectra.

Figure 4.1(d) compares the intensity of $612cm^{-1}$ mode for p and s polarized excitation. We chose $612cm^{-1}$ mode which is an in-plane C-C-C ring bending mode of R6G molecule. This choice was deliberate for two reasons: 1) This is the strongest mode in the recorded spectra; 2) The in-plane bending mode is compatible with polarization selection rules of SERS, and therefore ideal for testing polarization dependent SERS from anisotropic nanostructures such as isolated Ag NW ([33]). From Figure 4.1, it was evident that the p-polarized illumination resulted in higher intensity compared to s-polarized light. Motivated by the above observations, we explore two questions: (i) how do the SERS intensities vary as a function of input polarization (polarizer angle)? (ii) How do the SERS intensities vary as function of output polarization (analyzer angle) with the input polarization held constant?

### 4.1.1 Modulation of SERS intensity as function of input polarization

Figure A.0.3 shows variation of dark-field SERS intensity ($612cm^{-1}$ mode) from a single Ag NW as a function of input polarization without an analyzer. The polar plot is accompanied by the schematic of the experimental configuration. The plot shows that maximum intensity is obtained for incident polarization perpendicular to the nanowire axis, in this case, p polarized light and the minimum was obtained for s polarized light. This variation occurs because only Transverse Magnetic (TM) modes of surface plasmons exist. Transverse Electric (TE) modes cannot exist. The detailed proof for why this is so, can be found in the Appendix. Therefore, s polarized light cannot excite surface plasmons.

It was also evident that the dark-field SERS signal could be modulated by gradually varying the input polarization from p to s polarization. For all the angles between p and s polarized light, the field intensity was between the two extremes. Hence, this variation in electric field intensity is mapped to the resultant SERS intensity of single Ag NW, leading to modulation.

A relevant parameter in intensity modulation is the modulation depth (MD) given by

$$MD = \frac{I_{max} - I_{min}}{I_{max}} \tag{4.1}$$

where $I_{max}$ and $I_{min}$ are the maximum and minimum intensity obtained as function of variable polarization. For the data shown in Figure A.0.3(a), the MD was 0.88. This value, which is close to 1, indicates that: by systematically varying the input polarization to create evanescent fields, one can obtain large modulation in the resultant SERS signal. Such modulation capabilities

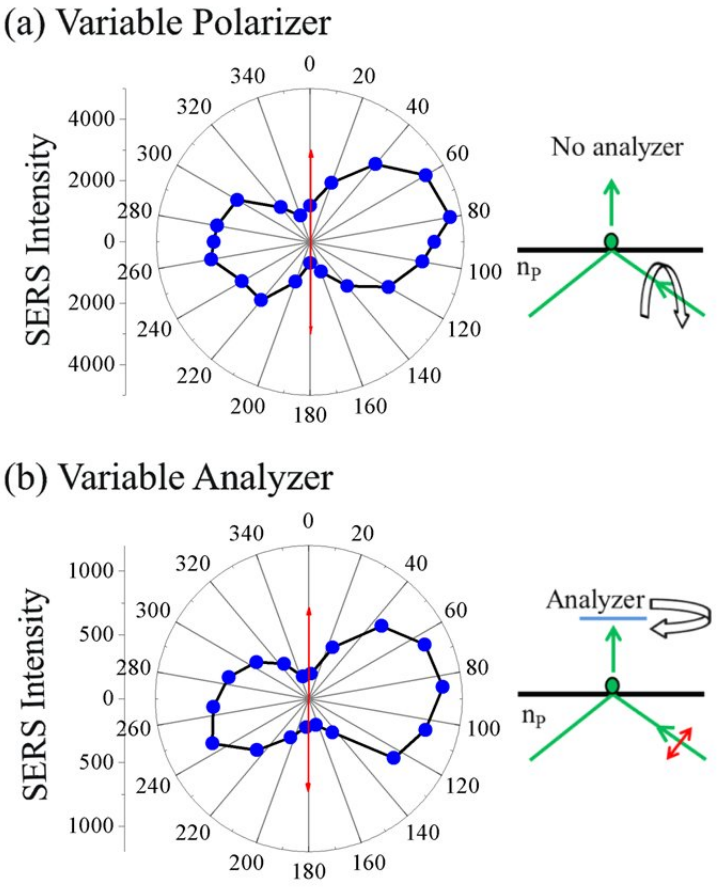


Figure 4.2: (a) Dark-field SERS intensity modulation from a single Ag NW as a function of input polarization angle (without an analyzer in the output path). Alongside, shown is the schematic of the experimental configuration; (b) Dark-field SERS intensity modulation from a single Ag NW as a function of analyzer angle with input excitation held at p polarization. Alongside, shown is the schematic of the experimental configuration. The arrows in polar plots indicate the orientation of Ag NW. The refractive index $n_p$ in the schematic represents the region of the prism.

are vital to control the interaction of molecular species with the localized electromagnetic field down to the nanoscale level.

### 4.1.2 Polarized SERS intensity as a function of output polarization

Further, we probed the output polarization characteristics of dark-field SERS signal for a constant input polarization. The input field was fixed at p-polarization, and the analyzer angle was varied. Figure A.0.3(b) shows the variation of dark-field SERS intensity from single Ag NW as a function output polarization. The plot is accompanied by the schematic of the experimental configuration. The arrow in the polar plot indicates the long-axis orientation of the nanowire. From the polar plot it was evident that maximum light was emitted in the direction perpendicular to the long-axis of the nanowire, and minimum was along the NW axis. The value of MD for this measurement was found to be 0.90, indicating a high modulation contrast in the output signal.

The electric field due to surface plasmons in a metal nanowire is polarized perpendicular to the wire ([1]). In other words, there is no component parallel to the wire. Therefore, the polarization of the scattered light from the wire is expected to be maximum in the direction perpendicular to the wire. The Raman scattered light from a molecule placed at the vicinity of a metal nanostructure gets enhanced due to the optical fields produced by the nanostructure. In addition, the Raman scattered light from the molecule gets further coupled to the nanostructure. Therefore, the polarization of the Raman scattered light is governed by the geometry of the wire, which explains why the light is highly polarized in the direction perpendicular to wire axis. Therefore, nanostructures act as potential nano-optical antennas ([32]).

### 4.1.3 SERS intensity modulation matrix as function of input and output polarization

The next question we asked was: how do the SERS intensities vary in the parameter space containing both input and output polarizations? To answer this, we performed multiple SERS measurements spanning various input and output polarization angles and created a SERS intensity matrix. Figure 4.1.3 shows modulation of SERS intensity by varying the input and output polarization angles. The maximum intensity was obtained for p-polarized input with analyzer angle oriented perpendicular to long axis of Ag NW and the minimum intensity was observed for s-polarized illumination with

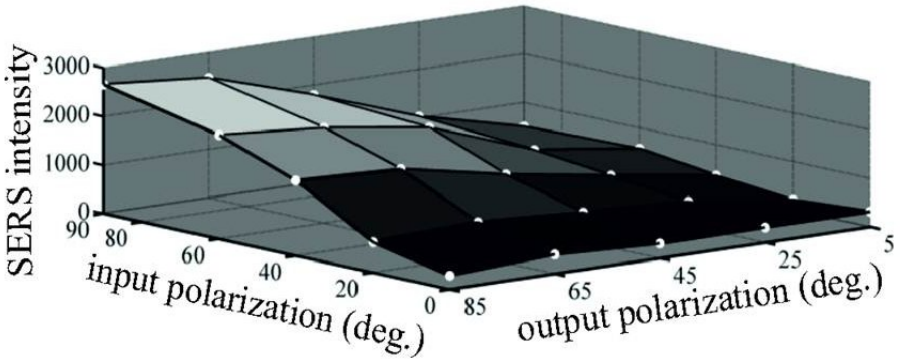


Figure 4.3: Dark-field SERS intensity modulation matrix from a single Ag nanowire as a function of input polarizer and output analyzer angles. The maximum intensity was observed for p polarized illumination with analyzer angle oriented perpendicular to the nanowire axis.

analyzer angle oriented parallel to nanowire axis. The matrix-data clearly indicates how SERS intensity can be systematically modulated by varying the angles of polarizer and analyzer. Such modulation will be of enormous use in single nanowire based-biosensors where the interaction between the local optical field and the biomolecules needs to be varied in a controlled way from a remote location.

Another interesting observation is the periodic intensity modulation in the dark-field Rayleigh images (Figure 4.1). Such intensity modulation has been observed previously ([17]) in lithographically fabricated nanowire structures, and occur due to plasmon beating phenomenon, where the interference between excited surface plasmon polariton and incident evanescent field interfere with each other giving rise to periodic fluctuation in intensity. For the current study, we have collected SERS signal from regions of maximum intensity.

Dark-field SERS was performed on a single Ag nanowire using total internal reflection geometry. The SERS intensity was modulated by varying the input polarization, and a modulation depth of 0.88 was observed. The output polarization from the SERS signal was resolved, and the maximum emission intensity was observed in the direction perpendicular to the long axis of the Ag NW. In contrast to point-scan illumination microscopy, the total internal reflection based Raman microscopy configuration, that we have discussed here, has advantage because the whole nanostructure is excited simultaneously using evanescent waves. Conventionally, single nanostructures

are optically excited using high numerical aperture objective lenses that may lead to photo-damage of either the nanostructure or the molecule coated on them. Our approach avoids this constraint by evanescent excitation and high numerical-aperture orthogonal collection. Another aspect of Ag NW is its ability to function as nano-optical waveguides. Therefore, the techniques discussed in this work can also be utilized in modulation of waveguiding characteristics and concomitantly harnessed for nano-optical sensing in miniaturized lab-on-chip environments.

## 4.2 Dark field Light Scattering from Nanoparticles

The non-propagating collective oscillations of the electrons in metal nanostructures are called Localized Surface Plasmons. The plasmon resonance frequencies of the nanoparticles lie in the visible region of light and depends on the size and shape of the particle. Therefore, nanoparticles display a variety of colors when illuminated in a dark-field configuration, due to resonantly enhanced absorption and scattering of light. Figures 4.5 and 4.4 show dark field microscope images of gold and silver nanoparticles of approximate sizes around 30nm and 60nm respectively.

### 4.2.1 Surface Plasmon Modes in Metallic Nanoparticles

Consider a nanoparticle of size $d$. For the case when $d \ll \lambda$, its interaction with light (of wavelength $\lambda$) can be described using simple quasi-static approximation. In this approximation, the particle is considered to be present in an electrostatic field, because the phase of the oscillating electromagnetic field (of light) is almost constant in the small volume occupied by the particle. This approximation gives good enough results for particles below 100nm. Assuming a perfectly spherical metal particle (of radius $a$ and described by an imaginary dielectric constant $\epsilon(\omega)$, present in a constant electric field given by $\mathbf{E}_0 = E_0\hat{\mathbf{z}}$ in a homogeneous medium of dielectric constant $\epsilon_s$, the electric field inside the particle can be found by first solving the Laplace equation $\bigtriangledown^2\Phi = 0$ for the potential $\Phi$. On using the Legendre Polynomial solution and putting in the appropriate boundary conditions, one obtains the following solution:

$$\Phi_{in} = -\frac{3\epsilon_s}{\epsilon + 2\epsilon_s} E_0 r cos\theta \tag{4.2a}$$

$$\Phi_{out} = -E_0 r cos\theta + \frac{\mathbf{p.r}}{4\pi\epsilon_0\epsilon_s r^3} \tag{4.2b}$$

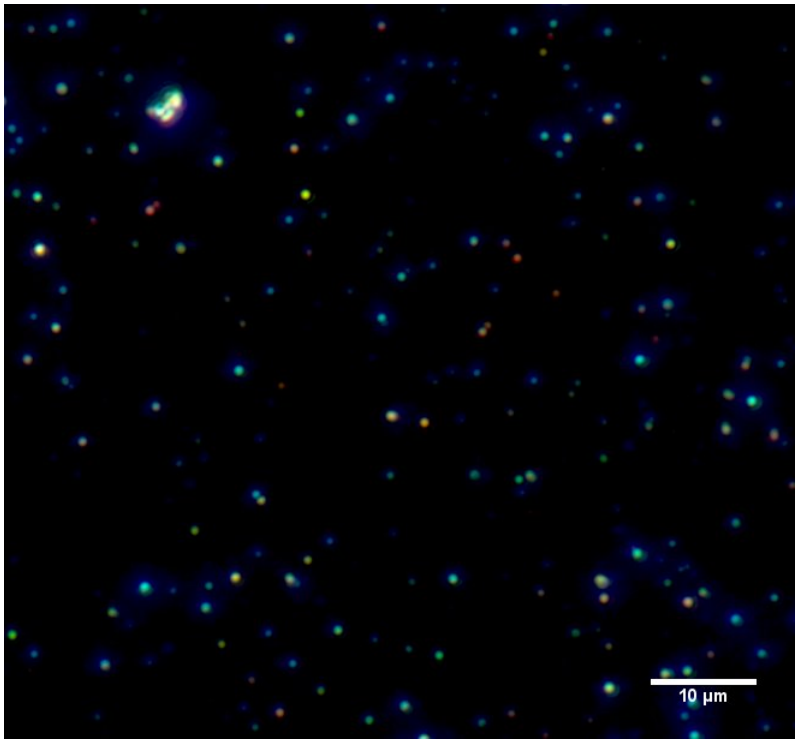


Figure 4.4: Silver Nanoparticles under Dark field illumination


Figure 4.5: Gold Nanoparticles under Dark field illumination

where,

$$\mathbf{p} = 4\pi\epsilon_0\epsilon_s a^3 \frac{\epsilon - \epsilon_s}{\epsilon + 2\epsilon_s}\mathbf{E}_0 \tag{4.2c}$$

$\mathbf{r}$ is the position vector of the point at which the field is being calculated. The second term in ((4.2c)) is like the potential due to a dipole located at the particle center. Therefore, we can say that the applied field induces a dipole moment in the particle with polarizability $\alpha$ (in $\mathbf{p} = \epsilon_0\epsilon_s\alpha\mathbf{E}_0$) given by:

$$\alpha = 4\pi a^3 \frac{\epsilon - \epsilon_s}{\epsilon + 2\epsilon_s} \tag{4.3}$$

The polarizability resonantly increases when $\mid \epsilon + 2\epsilon_s \mid$ is a minimum, i.e., when $Re[\epsilon(\omega)] = -2\epsilon_s$. Using $\mathbf{E} = -\bigtriangledown \Phi$, we obtain the following solution for the electric field:

$$\mathbf{E_{in}} = \frac{3\epsilon_s}{\epsilon + 2\epsilon_s}\mathbf{E}_0 \tag{4.4a}$$

$$\mathbf{E_{out}} = \mathbf{E}_0 + \frac{3\mathbf{n}(\mathbf{n}.\mathbf{p} - \mathbf{p})}{4\pi\epsilon_0\epsilon_s}\frac{1}{r^3} \tag{4.4b}$$

$\mathbf{n}$ is the normal vector. At resonance, the electric fields inside and outside the particle also increase greatly. This electric field enhancement is used for many applications in biosensors and detection - for example, such enhanced fields will be helpful for Surface enhanced Raman scattering studies. Under plane-wave illumination, i.e., if the incident electric field is given by $\mathbf{E} = \mathbf{E}_0 e^{-i\omega t}$, then the particle is induced with an oscillating dipole given by $\mathbf{p} = \epsilon_0\epsilon_s\alpha\mathbf{E}e^{-i\omega t}$. Consequently, the electric field resulting from the particle would be like the radiation from an oscillating dipole. The radiation of this dipole results in the scattering of the incident light. Although we won't go into the details of the exact form of the fields, one thing that is of interest here is the resonantly enhanced polarizability enhances the scattering and absorption cross sections of the nanoparticles. The following equations give the two cross sections:

$$C_{scat} = \frac{k^4}{6\pi}\alpha^2 \tag{4.5}$$

$$C_{abs} = kIm[\alpha] \tag{4.6}$$

As $\alpha$ depends on the radius of the particle as $a^3$, the scattering cross section changes with the sixth power of radius, whereas the absorption cross section changes with $a^3$. The sum of absorption and scattering is called extinction. Small gold particles absorb mostly in the green and near-blue light, therefore show red color and large gold particles scatter predominantly in green region and appear green. Using particles is usually more convinient in applications due to the large surface to volume ratio it offers.

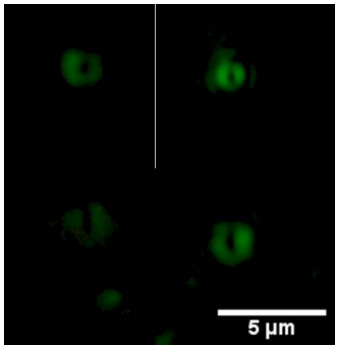


Figure 4.6: Simple Representation of a plasmonic NP interaction with gold film. The dipole parallel to the film is canceled out by the corresponding image dipole leaving only the Vertical Electric Dipole

## 4.3 Nanoparticles on thin films - Donut Modes

When nanoparticles are placed on thin film of metal (or any polarizable surface) and illuminated with light in dark field, we see a distinct donut-shaped electromagnetic field profile being emitted by the particle (Figure 4.6).

### 4.3.1 Vertical Electric Dipole

An image dipole of the metal nanoparticle is formed by the metal film. The horizontal component gets cancelled and only the vertical dipole remains. This results in an electric field shaped like two lobes around the particle, which makes it look like a donut ([10]). Figure 4.7 illustrates the phenomenon.

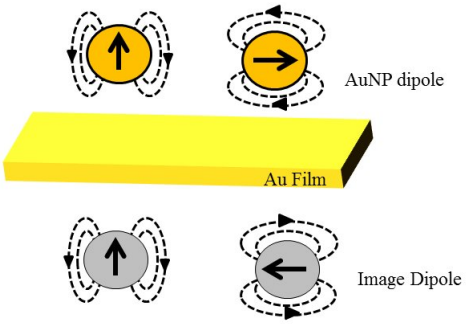


Figure 4.7: Simple Representation of a plasmonic NP interaction with gold film. The dipole parallel to the film is canceled out by the corresponding image dipole leaving only the Vertical Electric Dipole

# Chapter 5

# Optical Properties of Organic micro and nano-structures in evanescent field

In this chapter, we study the optical properties of organic micro/nanowires (made up of 1,5-diamino anthraquinone molecule) in an evanescent field, which is a result of their luminescent nature. We will first describe the experimental results obtained for these structures placed in an evanescent field. Further, we will discuss the possible explanations for the observations.

1,5-diamino anthraquinone is a planar molecule with two carbonyl and two amine groups. The molecules are stacked one on the other through interaction of their pi orbitals, during the formation of wires.

## 5.1 UV-Vis Spectal Characterization

The UV-Visible Absorption Spectra of individual DAAQ molecules (in solution) and the wires (in solid state) are shown in Figure 5.1. The two peaks at 300 nm and 480 nm in the monomers are due to the intramolecular charge transfer between the neighbouring amine and carbonyl groups of the molecule([50]). The UV-Vis absoprtion spectrum of the organic wires is clearly red shifted. The red shift in the absorption spectrum of the wires in comparison to the individual molecules is due to molecular aggregation. There are two types of molecular self assembly that are possible, owing to the strong intermolecular attraction in these aggregates ([31]). These aggregates show distinct changes (shifts) in their absorption spectra in comparison to that of the monomers: (1) Bathochromic shift (due to formation of J aggregates) and (2)hypsochromic shifts (due to formation of H aggregates).

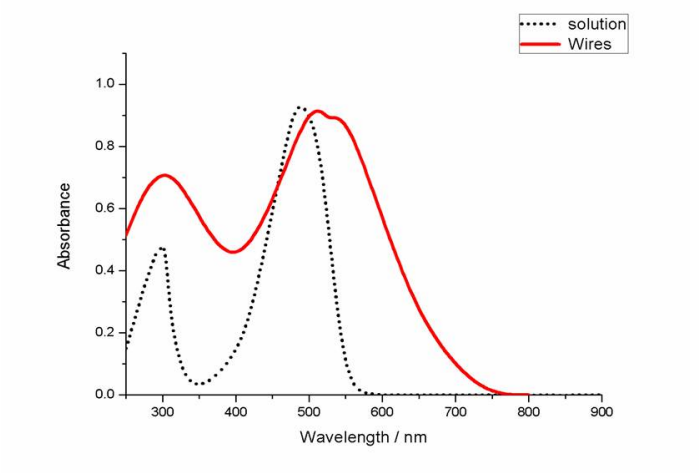


Figure 5.1: UV-Vis absorption spectra of DAAQ molecules and the wires

These two types of aggregation have been explained using molecular exciton coupling theory ([22]).

**H aggregates**: In the case of H aggregates, parallel plane-to-plane stacking occurs. Therefore, the transition dipoles of two molecules will be parallel to each other.

**J aggregates**: In the case of J aggregates, the molecules are connected head-to-tail (as shown in Figure 5.2). Therefore, the transition dipole moments are oblique to each other.

For both the cases, the energy level diagram is shown in Figure 5.2. Therefore, a transition to the upper state in case of the parallel transition dipole stacking leads to a hypsochromic (or blue) shift. A transition to a lower state in the case of the end-to-end stacking leads to a bathochromic (red) shift.

The 'angle of slippage' is used to distinguish between H-aggregated and J-aggregated bands. Angle of slippage is the angle between the axis containing the centers of the molecules and the long axis of any of the parallel molecules. For example, in Figure 5.2, the angle of slippage for the first illustration is $0^\circ$ and for the second case, it is somewhere between $0^\circ$ and $90^\circ$. For H-aggregates, the angle of slippage is less than $32^\circ$ and it is greater than $32^\circ$ for J-aggregated molecules.

In the organic wires, we see a red shift in the absorption spectrum in comparison to the monomer spectrum due to the molecular aggregation of the J-type. What one also notices is that the second peak in the absorption spectrum has split into two peaks. One is at 515 nm and the other is at 540 nm.

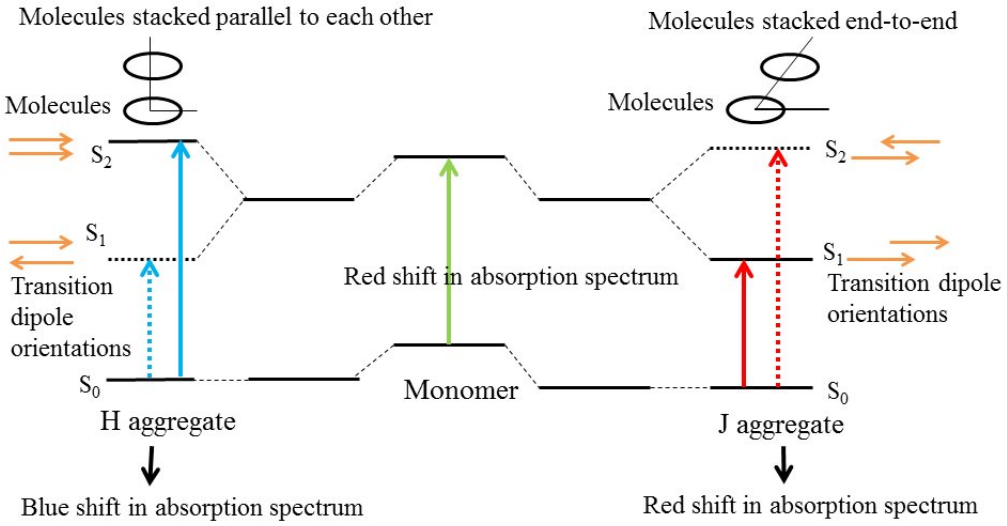


Figure 5.2: Simple representation of the types of stacking in molecular aggregates and the consequent shifts in the absorption spectra based on the molecular exciton theory

## 5.2 Exciton Polaritons

The J- band transitions behave in a similar way to crystals following the Frenkel exciton theory. An electronic transition from the $\pi \rightarrow \pi^*$ ([50]) leaves an electron-hole pair in the molecule, forming a Frenkel exciton. Frenkel excitons in organic crystals have an excitation energy ($E_{ex}$) of the order of an eV ([42]). This exciton emits a photon which in turn excites an exciton in the adjacent molecule. This way the exciton 'hops' from molecule to molecule, thus making the organic wires active waveguides. In other words, the molecules absorbs and re-emits the photon at each step during the propagation of light. Therefore, the light propagation in organic wires is due to Exciton Polaritons. The waveguiding nature is illustrated clearly in Figure 5.3.

## 5.3 Polarization dependent Photoluminescence

Organic wires are placed in the evanescent field created on the dove prism and the photo luminescence spectrum was collected for various input polarizations. Photoluminescence is a process where a material, upon excitation by light, re-emits radiation at a different wavelength. For photoluminescence

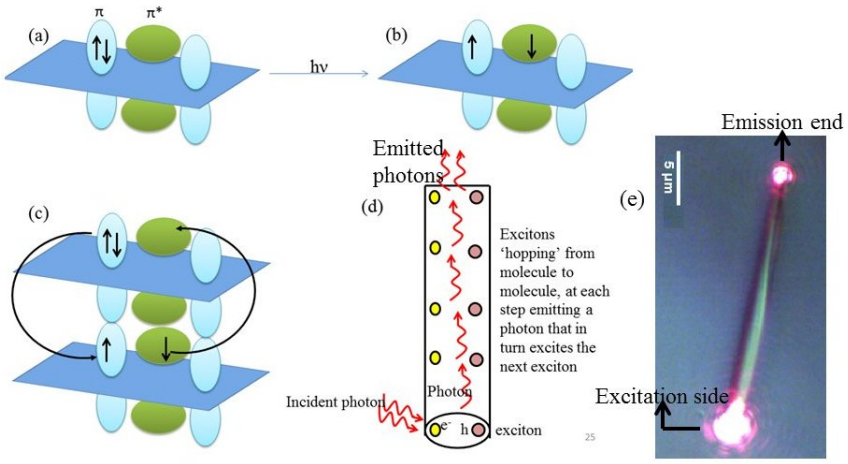


Figure 5.3: (a) Illustration of the orbitals and electrons in a single molecule, (b) The transition from $\pi$ to $\pi^*$ gives rise to an electron-hole pair (exciton), (c) Illustration of how the exciton gets transferred to neighboring molecule, (d) Illustration of how active waveguiding occurs in these wires, (e) Light propagation shown in an organic wire. The wire is illuminated at the bottom end and one can see the light being emitted from the other end.

to occur, light must be provided at a frequency equal to or more than the band gap of the material that is being excited. Upon absorption of this light, an electron is excited to the conduction band from the valence band (electron hole pair is created). The electron is excited to energy states high up in the conduction band. The electron relaxes within 0.1 picoseconds to the lowest energy state of the conduction band through non-radiative decay. The electron then returns to the valence band by the emission of photon - Photoluminescence (PL). Evidently, the energy of this light will be lesser than that of the incident excitation light.

In all our experiments, the organic wires were excited using laser light of 532nm and the PL was collected from 550nm to 1000nm. Also, in our studies, we are interested in studying the PL properties of single isolated wires (unlike the studies of bulk sample of wires that are reported in [50]).

The photoluminescence spectrum of a single wire exhibits a broad band ranging from 550 nm upto 800 nm. Upon excitation with evanescent field, it was seen that the photoluminescence band shifts from lower wavelength to higher wavelength as the polarization of the incident light is changed from p to s. The shift is clearly illustrated in Figure 5.5. From the inset (which is just an enlarged version of a part of the spectra), one can see that the shift happens over a range of nearly 30nm.

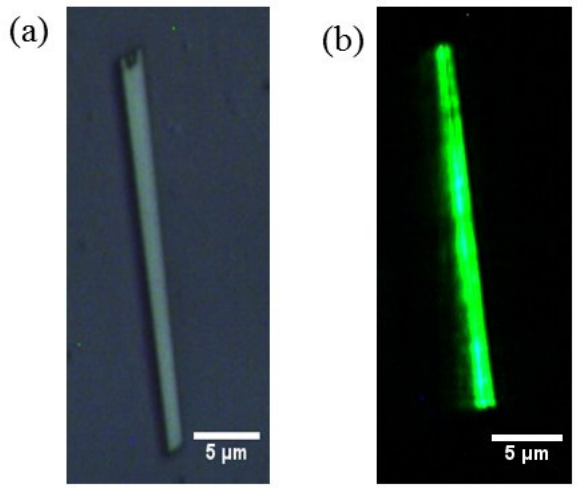


Figure 5.4: (a) Bright field image, (b) TIR Dark Field Rayleigh scattering image of single isolated Organic wire

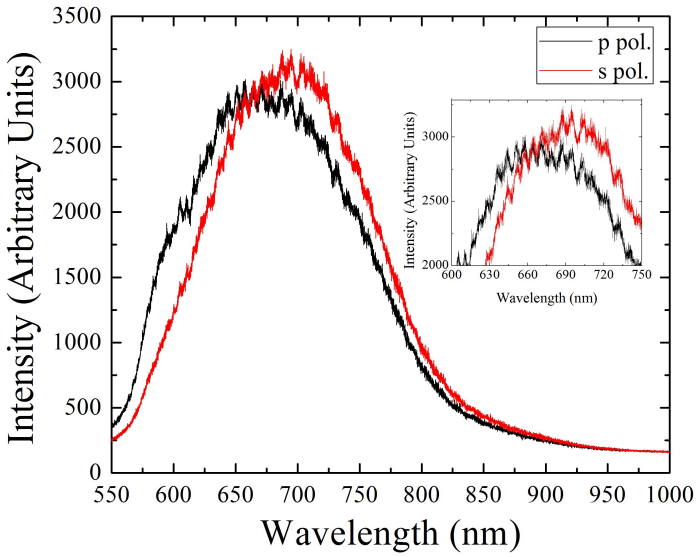


Figure 5.5: PL spectra of a single organic wire under evanescent field of two different polarizations

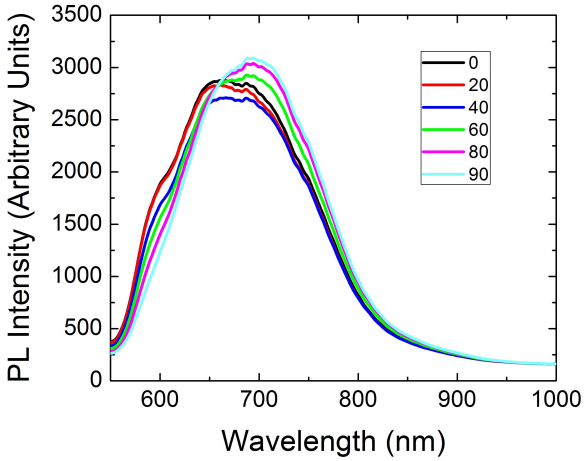


Figure 5.6: The gradual shift in PL from a single isolated organic wire as polarization of incident light is changed from '0' representing p polarization to '90' representing s polarization. All the other numbers correspond to the angle the direction of polarization makes with respect to that of p polarization.

The periodic fine structures observed in the spectra are a result of Fabry-Perot resonances in the wire ([3]) Further, we saw that the shift occurs gradually as one goes from s to p polarizations, by changing the angle of polarization direction with respect to the in steps of 20°. This is clearly seen in Figure 5.6. The plots have been smoothened in order to remove the fine structure, so that comparison becomes easier and more clear.

In the next step, we checked whether a similar effect is seen using point illumination from the top through the objective lens. Laser light is focused at a point on the wire through the objective lens which also collects the back scattered light that is sent into the spectrometer. There are two polarizations that are possible using this type of illumination - parallel to the wire and perpendicular to the wire within the same x-y plane. Interestingly, we did not observe any effect of the polarization of the top-illumination on the PL obtained from the wire, as shown in Figure 5.7. In the same figure, PL spectra obtained using top illumination and from evanescent field of two different polarizations are plotted all together for the sake of comparison.

### 5.3.1 Discussion

We saw that the photoluminescence signal band from a single isolated organic wire placed in a TIR evanescent field shifts considerably upon change

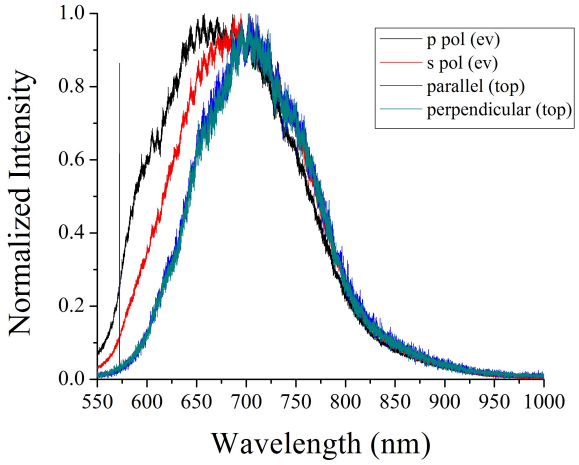


Figure 5.7: PL spectra obtained from single organic wire using evanescent illumination (s and p pol.) and focused point illumination from objective with electric fields parallel [parallel (top)] and perpendicular [perpendicular (top)] to the wire's long axis. As is evident, the PL shift upon change of incident light polarization is not seen in case of the second form of illumination (from top).

in polarization of incident light from p to s. This kind of shift does not occur upon point illumination from the top through an objective lens. Using evanescent coupling, we are illuminating the entire wire (and not just a single point). In addition, the p polarized evanescent field has its electric field in the z direction, and this cannot be achieved using point illumination from the top. Therefore, one could speculate that excitation of entire wire simultaneously and excitation of a different absorption band by the p polarized evanescent field could be the reasons for the observed shift. Further evidence for the formation of different band structures in the wire, as compared to the molecule can be obtained from the UV-Vis absorption spectrum for the wire, where the second peak was observed to split into two. However, the UV-Vis spectrum is an ensemble average of the absorption from many wires, whereas the PL spectrum is taken from a single isolated wire. Hence, we cannot consider this as conclusive evidence. Further work will be focused on understanding the reasons behind the observed phenomenon.

All the results shown here are for wires oriented in the y direction. Wires oriented along the x direction show scattering/emission only at one end. Wires oriented at any angle between x and y sometimes show illumination at two ends. Therefore, the wire orientation plays a critical role in its interaction with the evanescent field. Therefore, a detailed study in this regard might be

quite useful. Also, from the point of view of applications, it is important that we have control over the orientation of all the wires in the sample. Vertically grown (perpendicular to the plane of the substrate) nanowires have been shown to have numerous applications. We can use evanescent coupling for simultaneous excitation of an array of vertical nanowires, which then couple this near field light to the far field through emission from the other end.

The unique feature of evanescent excitation is, as mentioned earlier, the electric field in z direction. It is necessary to study samples under z polarization excitation. This is not always possible with microscopy systems, because incident light (k vector) is in z direction. We have already seen that this gives rise to some interesting PL properties in organic wires. Since this could be a geometry dependent phenomenon, one should expect such a shift in PL even with wires made up of other molecules. Organic molecule lasers have been built using various techniques such as two-photon fluorescence ([49]). One way to achieve tune-ability in those lasers is through excitation using evanescent fields with varying polarizations. The wires now act as optical cavities (due to their waveguiding nature). Further work would be required to actually achieve considerable population inversion and coherence and make the wires potential laser sources.

# References


[1] *Principles of Nano-Optics*. Cambridge University Press, 2006.

[2] *Plasmonics: Fundamentals and Applications*. Springer, New York, 2007.

[3] *Optics*. Pearson, 2008.

[4] Y. Xia A. Chen A. L. Pyayt, B. Wiley and L. Dalton. Integration of photonic and silver nanowire plasmonic waveguides. *Nature Nanotechnology*, 3:660–665, 2008.

[5] Jeffrey N. Anker, W.Paige Hall, Olga Lyandres, Nilam C. Shah, Jing Zhao, and Richard P. Van Duyne. Biosensing with plasmonic nanosensors. *Nature Materials*, 7(6):442–453, 2008.

[6] D. Axelrod, T. P. Burghardt, and N. L. Thompson. Total internal reflection fluorescence. *Annual review of biophysics and bioengineering*, 13:247–268, 1984.

[7] Carl J. Barrelet, Andrew B. Greytak, and Charles M. Lieber. Nanowire photonic circuit elements. *Nano Letters*, 4(10):1981–1985, 2004.

[8] David C. S. Beddows, Ben C. Griffiths, Ota Samek, and Helmut H. Telle. Application of frustrated total internal reflection devices to analytical laser spectroscopy. *Applied Optics*, 42(30):6006–6015, 2003.

[9] Paul R. Berman. Goos-haenchen effect. *Scholarpedia*, 7(3):11584, 2012.

[10] S. Y. Chen, J. J. Mock, R. T. Hill, A. Chilkoti, D. R. Smith, and A. A. Lazarides. Gold nanoparticles on polarizable surfaces as raman scattering antennas. *ACS Nano*, 4:6535–6546, 2010.

[11] Jenny Clark and Guglielmo Lanzani. Organic photonics for communications. *Nature Photonics*, 2010.

[12] Ian N. Court and Frederick K. von Willisen. Frustrated total internal reflection and application of its principle to laser cavity design. *Applied Optics*, 3(6):719–726, 1964.

[13] Qiu Hong Cui, Yong Sheng Zhao, and Jiannian Yao. Photonic applications of one-dimensional organic single-crystalline nanostructures: optical waveguides and optically pumped lasers. *Journal of Materials Chemistry*, 2012.

[14] Andreas; Wagner Dieter; Kreibig Uwe; Rogers Michael; Hofer Ferdinand; Aussenegg Franz R.; Krenn Joachim R. Ditlbacher, Harald; Hohenau. Silver nanowires as surface plasmon resonators. *Physical Review Letters*, 95(25):257403/1–257403/4, 2005.

[15] T. W. Ebbesen, C. Genet, and S. I. Bozhevolnyi. Surface-plasmon circuitry. *Physics Today*, 61:44–50, 2008.

[16] Y. Fang, H. Wei, F. Hao, P. Nordlander, and H. Xu. Remote-excitation surface-enhanced raman scattering using propagating ag nanowire plasmons. *Nanoletters*, 9:2049–2053, 2009.

[17] N. Felidj, G. Laurent, J. Grand, J. Aubard, G. Levi, A. Hohenau, F. R. Aussenegg, and J. R. Krenn. Far-field raman imaging of short-wavelength particle plasmons on gold nanorods. *Plasmonics*, 1:35–39, 2006.

[18] Richard P. Feynmann. There's plenty of room at the bottom. *Engineering and Science*, 1960.

[19] Naomi J. Halas, Surbhi Lal, Wei-Shun Chang, Stephan Link, and Peter Nordlander. Plasmons in strongly coupled metallic nanostructures. *Chemical Reviews*, 111(6):3913–3961, 2011.

[20] Russell J. Holmes. Optical materials: Nanowire lasers go organic. *Nature Nanotechnology*, 2(3):141–142, 2007.

[21] J. A. Hutchison, S. P. Centeno, H. Odaka, H. Fukumura, J. Hofkens, and H. Uji-i. Subdiffraction limited, remote excitation of surface enhanced raman scattering. *Nanoletters*, 9:995–1001, 2009.

[22] M. Kasha, H. R. Rawis, and M. A. El-Bayoumi. The exciton model in molecular spectroscopy. *Pure Appl. Chem.*, 1965.

[23] Mark W. Knight, Nathaniel K. Grady, Rizia Bardhan, Feng Hao, Peter Nordlander, and Naomi J. Halas. Nanoparticle-mediated coupling of light into a nanowire. *Nano Letters*, 7(8):2346–2350, 2007.

[24] S. Lal, J. H. Hafner, N. J. Halas, S. Link, and P. Nordlander. Noble metal nanowires: From plasmon waveguides to passive and active devices. *Accounts of Chemical Research*, 45(1887-1895), 2012.

[25] Stephan; Halas Naomi J. Lal, Surbhi; Link. Nano-optics: From sensing to waveguiding. *Nature Photonics*, 1(11):641–648, 2007.

[26] Surbhi Lal, Nathaniel K. Grady, Janardan Kundu, Carly S. Levin, J. Britt Lassiter, and Naomi J. Halas. Tailoring plasmonic substrates for surface enhanced spectroscopies. *Chem. Soc. Rev.*, 37:898–911, 2008.

[27] Matt Law, Donald J. Sirbuly, Justin C. Johnson, Josh Goldberger, Richard J. Saykally, and Peidong Yang. Nanoribbon waveguides for subwavelength photonics integration. *Science*, 305(5688):1269–1273, 2004.

[28] P.C. Lee and D. Meisel. Adsorption and surface-enhanced raman of dyes on silver and gold sols. *Journal of Physical Chemistry*, 86(17):3391–3395, 1982.

[29] C. D. Mellor, C. D. Bain, and J. Lekner. Pattern formation in evanescent wave optical traps. *Proceedings of SPIE âĂŞ The International Society for Optical Engineering*, 5930:352–361, 2005.

[30] C.D. Mellor and C.D. Bain. Array formation in evanescent waves. *ChemPhysChem*, 7(2):329–332, 2006.

[31] Amaresh Mishra, Rajani K. Behera, Pradipta K. Behera, Bijaya K. Mishra, and Gopa B. Behera. Cyanines during the 1990s: A review. *Chemical Reviews*, 2000.

[32] Martin Moskovits. Surface-enhanced spectroscopy. *Reviews of Modern Physics*, 1985.

[33] A. Pal, S. Gohil, S. Ghosh, and P. Ayyub. Polarization selection rules for surface-enhanced raman scattering from anisotropic microstructured surfaces. *Journal of Physical Chemistry C*, 2012.

[34] Nilam C. Shah Paul L. Stiles, Jon A. Dieringer and Richard P. Van Duyne. Surface-enhanced raman spectroscopy. *Annual Review of Analytical Chemistry*, 1:601–626, 2008.

[35] M. Pelton, J. Aizpurua, and G. Bryant. Metal-nanoparticle plasmonics. *Laser and Plasmonics Reviews*, 2(3):136–159, 2008.

[36] Frank Pillon, Herve Gilles, and Sylvain Girard. Experimental observation of the imbertâĂŞfedorov transverse displacement after a single total reflection. *Applied Optics*, 2004.

[37] Romain Quidant. Plasmonic tweezersâĂŤthe strength of surface plasmons. *MRS Bulletin*, 37:739–744, 2012.

[38] David A.; Wiley Benjamin J.; Xia Younan; Dufresne Eric R.; Reed Mark A. Sanders, Aric W.; Routenberg. Observation of plasmon propagation, redirection, and fan-out in silver nanowires. *Nano Letters*, 6(8):1822–1826, 2006.

[39] Donald J. Sirbuly, Matt Law, Haoquan Yan, and Peidong Yang. Semiconductor nanowires for subwavelength photonics integration. *The Journal of Physical Chemistry B*, 109(32):15190–15213, 2005.

[40] Volker J. Sorger, Rupert F. Oulton, Ren-Min Ma, and Xiang Zhang. Toward integrated plasmonic circuits. *MRS Bulletin*, 37:728–738, 7 2012.

[41] Y. Sun, B. Gates, B. Mayers, and Y. Xia. Crystalline silver nanowires by soft solution processing. *Nanoletters*, 2:165–168, 2002.

[42] Ken Takazawa, Jun ichi Inoue, Kazutaka Mitsuishi, and Tadashi Takamasu. Fraction of a millimeter propagation of exciton polaritons in photoexcited nanofibers of organic dye. *Physical Review Letters*, 2010.

[43] Lambert K. van Vugt, Sven RÃijhle, and DaniÃńl Vanmaekelbergh. Phase-correlated nondirectional laser emission from the end facets of a zno nanowire. *Nano Letters*, 6(12):2707–2711, 2006. PMID: 17163692.

[44] W. Wang, Q. Yang, F. Fan, H. Xu, and Z. L. Wang. Light propagation in curved silver nanowire plasmonic waveguides. *Nanoletters*, 11:1603–1608, 2011.

[45] H. Wei, Z. Wang, X. Tian, M. Kall, and H. Xu. Cascaded logic gates in nanophotonic plasmon networks. *Nature Communications*, 2:387, 2011.

[46] Hong Wei, Daniel Ratchford, Xiaoqin (Elaine) Li, Hongxing Xu, and Chih-Kang Shih. Propagating surface plasmon induced photon emission from quantum dots. *Nano Letters*, 9(12):4168–4171, 2009. PMID: 19821597.

[47] H. Yan, J. Johnson, M. Law, R. He, K. Knutsen, J.R. McKinney, J. Pham, R. Saykally, and P. Yang. Zno nanoribbon microcavity lasers. *Advanced Materials*, 15(22):1907–1911, 2003.

[48] Anatoly V. Zayats, Igor I. Smolyaninov, and Alexei A. Maradudin. Nano-optics of surface plasmon polaritons. *Physics Reports*, 408:131 – 314, 2005.

[49] Chuang Zhang, Yong Sheng Zhao, and Jiannian Yao. Optical waveguides at micro/nanoscale based on functional small organic molecules. *Phys. Chem. Chem. Phys.*, 2011.

[50] Yong Sheng Zhao, Jinsong Wu, and Jiaxing Huang. Vertical organic nanowire arrays: Controlled synthesis and chemical sensors. *JACS Communications*, 2009.

# Appendix A

# Surface Plasmon Polaritons

In this appendix, we will first introduce the surface plasmon wave equation, the dispersion relation for the SPPs, the Prism coupling method of excitation of surface plasmons and finally why surface plasmon modes can only be transverse magnetic (TM) and not transverse electric (TE).

### A.0.2 Wave Equation for SPPs

Lets consider a simple geometry consisting of a dielectric - metal interface. In the absence of external charge and current, the electromagnetic wave equation is given as:

$$\bigtriangledown^2 \mathbf{E} - \frac{\epsilon}{c^2}\frac{\partial^2 \mathbf{E}}{\partial t^2} = 0 \tag{A.1}$$

This equation has to be solved separately in the two regions of constant $\epsilon$ (the metal and the dielectric) and then the two solutions are combined by using boundary conditions. Without loss of generality, one can assume the solution to be of the form $\mathbf{E}(\mathbf{r}, t) = \mathbf{E}(\mathbf{r})e^{-i\omega t}$. Upon inserting this solution into (A.1), one gets

$$\bigtriangledown^2 \mathbf{E} + \left(\frac{\omega}{c}\right)^2 \epsilon \mathbf{E} = 0 \tag{A.2}$$

Take $\frac{\omega}{c} = k_0$. Lets take a cartesian coordinate system where the wave propagates in the x direction, y is the in-plane direction perpendicular to the x direction (and hence no change in $\epsilon$ along the x and y axes). Therefore, $\epsilon$ varies only in the z direction, with $z = 0$ representing the interface. Therefore,

$$\mathbf{E}(x, y, z) = \mathbf{E}(z)e^{iKx} \tag{A.3}$$

Inserting this in (A.2), we obtain:

$$\frac{\partial^2 \mathbf{E}(z)}{\partial z^2} + (k_0^2\epsilon - K^2)\mathbf{E} = 0 \tag{A.4}$$

(A.4) gives the final wave equation for in general, any electromagnetic mode in waveguides. A similar equation exists for the magnetic field as well. We need to find more explicit expressions giving relations between the different components of $\mathbf{E}$ and $\mathbf{B}$, before being able to solve the wave equation. For this, we use the two Maxwell's equations given as follows:

$$\bigtriangledown \times \mathbf{E} = -\frac{\partial \mathbf{B}}{\partial t} \tag{A.5}$$

$$\bigtriangledown \times \mathbf{H} = \frac{\partial \mathbf{D}}{\partial t} \tag{A.6}$$

We break both the equations down component wise and use all of the following conditions: Considering linear media, we have $\mathbf{D} = \epsilon \mathbf{E}$ and $\mathbf{B} = \mu_0 \mathbf{H}$. From the assumption of harmonic time dependence of the electric and magnetic field, we can write $\frac{\partial (E,B)_i}{\partial t} = -i\omega(E,B)_i$. Also, since there is no variation of electric field or magnetic field in the direction of y axis, $\frac{\partial}{\partial t} = 0$. In addition, from (A.3), we obtain $\frac{\partial}{\partial y} = iK$. Using all these, we get,

$$\frac{\partial E_y}{\partial z} = -i\omega\mu_0 H_x \tag{A.7a}$$

$$\frac{\partial E_x}{\partial z} - iKE_z = i\omega\mu_0 H_y \tag{A.7b}$$

$$iKE_y = i\omega\mu_0 H_z \tag{A.7c}$$

$$\frac{\partial H_y}{\partial z} = i\omega\epsilon_0\epsilon E_x \tag{A.7d}$$

$$\frac{\partial H_x}{\partial z} = -i\omega\epsilon_0\epsilon E_y \tag{A.7e}$$

$$iKH_y = -i\omega\epsilon_0\epsilon E_z \tag{A.7f}$$

Since electric and magnetic fields in electromagnetic waves are perpendicular to each other and to the propagation vector in homogeneous isotropic media, it is evident that two sets of solutions only are possible: Transverse Magnetic (TM or p) modes with non-zero $E_x$, $E_z$ and $H_y$ and Transverse Electric (TE or s) modes with non zero $H_x, H_z and E_y$. In summary, the governing equations for TM Modes are given as:

$$E_x = -i\left(\frac{1}{\omega\epsilon_0\epsilon}\right)\frac{\partial H_y}{\partial z} \tag{A.8a}$$

$$E_z = -\frac{K}{\omega\epsilon_0\epsilon}H_y \tag{A.8b}$$

$$\frac{\partial^2 H_y}{\partial z^2} + (k_0^2\epsilon - K^2)H_y = 0 \tag{A.8c}$$

The governing equations for TE Modes are given as:

$$H_x = i\left(\frac{1}{\omega\mu_0}\right)\frac{\partial E_y}{\partial z} \tag{A.9a}$$

$$H_z = \frac{K}{\omega\mu_0}E_y \tag{A.9b}$$

$$\frac{\partial^2 E_y}{\partial z^2} + (k_0^2\epsilon - K^2)E_y = 0 \tag{A.9c}$$

Let us get back to the geometry we have considered, where there is a dielectric half space ($z > 0$) with positive real dielectric constant ($\epsilon_2$) and an adjacent conducting (metal) half space ($z < 0$) with imaginary dielectric constant that depends on the frequency ($\epsilon_1(\omega)$) with $Re[\epsilon_1] < 0$ as is required for metals. Since we are interested in interface waves that propagate in x direction and evanescently decay in the z direction, we can write:

$$H_{y,2}(z) = A_2 e^{iKx}e^{-k_2 z} \tag{A.10a}$$

$k_2$ is the component of wave vector perpendicular to the interface in the dielectric medium. $1/k_1$ gives the decay length of the z component in the metal medium. And using (A.8a) and (A.8b), we obtain

$$E_{x,2}(z) = iA_2\left(\frac{1}{\omega\epsilon_0\epsilon_2}\right)k_2 e^{iKx}e^{-k_2 z} \tag{A.10b}$$

and

$$E_{z,2}(z) = -A_1\left(\frac{K}{\omega\epsilon_0\epsilon_2}\right)e^{iKx}e^{-k_2 z} \tag{A.10c}$$

for $z > 0$, i.e., for dielectric medium.

Similarly, for the metal medium ($z < 0$), the electric and magnetic fields are given as:

$$H_{y,1}(z) = A_1 e^{iKx}e^{k_1 z} \tag{A.11a}$$

$k_1$ is the component of wave vector perpendicular to the interface in the dielectric medium. $1/k_1$ gives the decay length of the z component in the metal medium.

$$E_{x,1}(z) = -iA_1\left(\frac{1}{\omega\epsilon_0\epsilon_1}\right)k_1 e^{iKx}e^{k_1 z} \tag{A.11b}$$

$$E_{z,1}(z) = -A_1\left(\frac{K}{\omega\epsilon_0\epsilon_2}\right)e^{iKx}e^{k_1 z} \tag{A.11c}$$

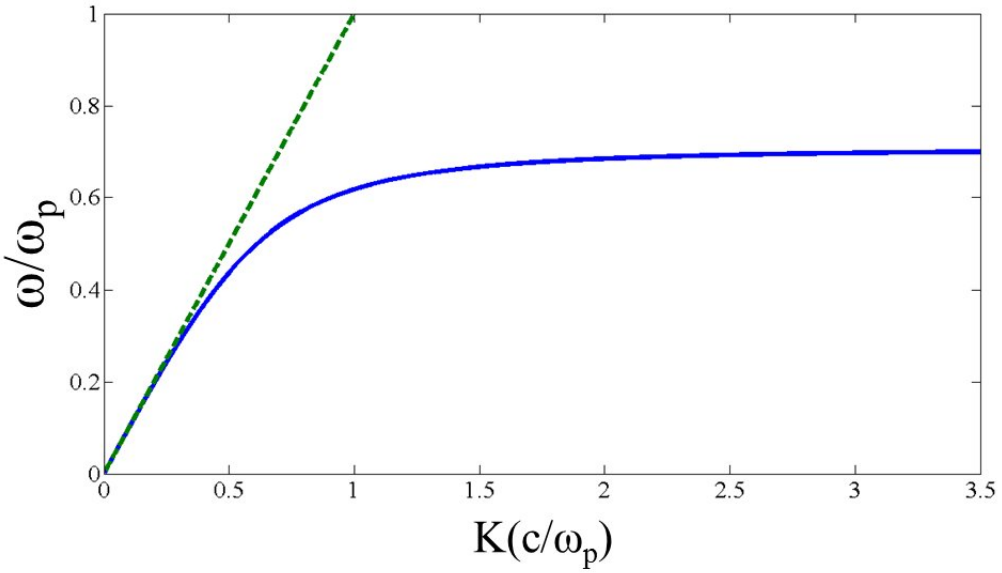


Figure A.1: Blue: Dispersion relations for the metal (following Drude Model) and Green: Light Line for air medium

The Maxwell's boundary conditions require that (i)$H_{y,1} = H_{y,2}$, (ii) $\epsilon_1 E_{z,1} = \epsilon_2 E_{z,2}$ and (iii) $E_{x,1} = E_{x,2}$. From (i) and (ii), we obtain $A_1 = A_2$. From (iii), we obtain

$$\frac{k_2}{\epsilon_2} = -\frac{k_1}{\epsilon_1} \tag{A.12}$$

This derivation is general and we never used the fact that one of the media is a metal and the other is a dielectric. But since $k_1$ and $k_2$ should be positive (for the waves to decay in the z direction in both the media) and $\epsilon_2$ is positive, it is required that $Re[\epsilon_1] < 0$, i.e., such surface waves exist only at metal-dielectric interface. Since the expressions for $H_y$ ((A.10a) and (A.11a)) should satisfy the wave equation (A.8c), we obtain,

$$k_1^2 = K^2 - k_0^2 \epsilon_1 \tag{A.13a}$$

$$k_2^2 = K^2 - k_0^2 \epsilon_2 \tag{A.13b}$$

From (A.12), (A.13a) and (A.13b), we get

$$K = k_0 \left( \frac{\epsilon_1 \epsilon_2}{\epsilon_1 + \epsilon_2} \right)^{1/2} \tag{A.14}$$

Remember that $k_0 = \frac{\omega}{c}$ and K is the wave vector for the SPP. Therefore, (A.14) gives the dispersion relation for a SPP. Assuming metals follow a

simple Drude's Model, the frequency dependent dielectric constant is given as:

$$\epsilon(\omega) = 1 - \frac{\omega_p^2}{\omega^2 + i\gamma\omega} \tag{A.15}$$

where $\omega_p = (ne^2/\epsilon_0 m)^{1/2}$ is called the bulk plasma frequency (n is the electron density) and $\gamma = 1/\tau$ is the collision frequency and $\tau$ is the relaxation time. The real and imaginary parts separately, of this $\epsilon(\omega)$ are given as:

$$Re[\epsilon(\omega)] = 1 - \frac{\omega_p^2\tau^2}{1 + \omega^2\tau^2} \tag{A.16a}$$

$$Im[\epsilon(\omega)] = \frac{\omega_p^2\tau^2}{\omega(1 + \omega^2\tau^2)} \tag{A.16b}$$

Metallic charater is retained for $\omega < \omega_p$. For $\omega$ close to $\omega_p$, $\omega\tau \gg 1$ and therefore, the imaginary part of dielectric constant (which actually signifies the damping) can be considered negligible. Therefore, we can write

$$\epsilon(\omega) = 1 - \frac{\omega_p^2}{\omega^2} \tag{A.17}$$

Insert this in (A.14) and plot the SPP dispersion relation for an air-silver metal interface. See figure A.1 for SPP dispersion and the dispersion relation for plane light wave on the air side (the light line). As is evident from the figure, the dispersion for the SPP lies to the right of the light line. For no frequency, the k vectors (and hence the momentum $\hbar k$) can be matched between the two for the given geometry of a single dielectric-metal interface. So alternate phase-matching conditions have to be used to excite plasmons. One of them is the prism coupling method.

Before we go on to discuss how the prism configuration can be used to excite plasmons, it should be mentioned here that the dielectric constant of metal given by (A.17) is assuming the metals follow simple Drude Model (with negligible damping). Real metals do not exactly follow this model for all the ranges of frequencies. We shall consider noble metals such as gold, silver because they are the ones that are usually used for plasmonic studies. The discrepancy in the Drude Model occurs because in noble metals, interband transitions occur at visible and near infrared frequencies. There will be transitions from the sp band to the d bands. However, these interband transitions can be described classically by just adding an additional term that describes the electron as bound to the positive ion core, i.e., by adding an additional restoring force term to the original differential equation for motion of the electron used in the Drude Model. This additional term then gives rise

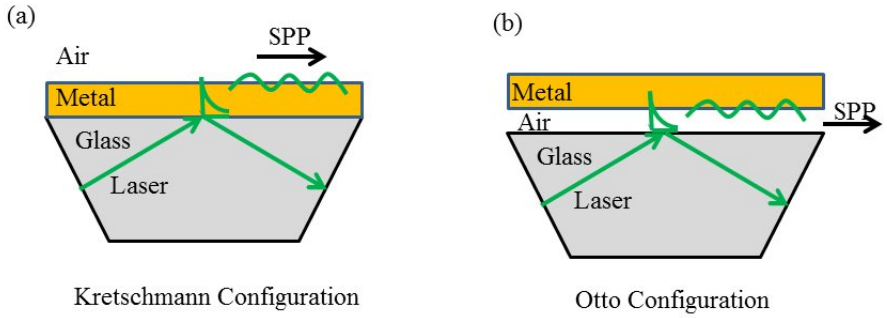


Figure A.2: Two ways to excite surface plasmons on a thin Metal film: (a) Kretschmann Configuration (b) Otto Configuration

to a resonance frequency for the electron. This is solved for obtaining the modified dielectric constant. However, the essential physics to describe how SPP coupling happens is all contained and can be explained satisfactorily using just the Drude Model. For the sake of completion, the following figure gives the actual dispersion relations for metals.

### A.0.3 Prism Coupling

Prism coupling method uses a three-layer system (instead of a simple metal-dielectric two layer interface). There are two types of Prism coupling configurations: (i) Kretschmann Configuration (the one used in our experiments) and (ii) Otto Configuration. Both the configurations are shown in Figure A.2.

### A.0.4 Kretschmann Configuration

This configuration consists of thin metal layer sandwiched between two dielectrics of different dielectric constants. Light wave is total internally reflected at the prism-metal interface giving rise to evanescent waves, that will result in the metal attaining an in-plane momentum of $k_x = k\sqrt{\epsilon}sin\theta$, which is enough to excite SPPs at the metal-air interface. That is, since the metal-air dispersion relation lies between that of the light line for prism and air, it is possible to excite plasmons there. Notice that plasmons still cannot be excited at the metal-prism interface (since dispersion for prism-metal interface lies to the left of the light line for prism). See Figure A.3. In the Otto configuration also, TIR takes place at the air-prism interface giving rise to evanescent waves which 'tunnel' through the small air gap and excite SPPs

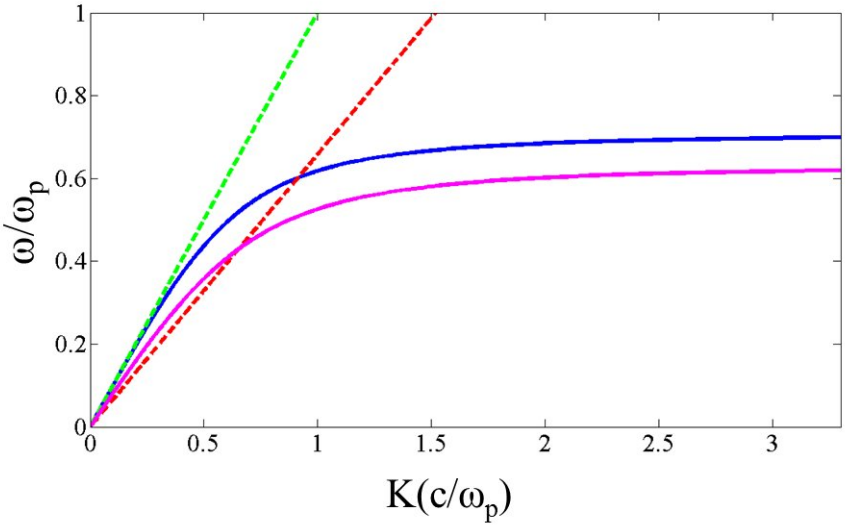


Figure A.3: Blue: Dispersion relations for the metal(Ag)-air interface (Metal described by Drude Model); Green: Light Line for air medium; Red: Light Line for prism (glass) medium; Magenta: Dispersion relation for metal-prism interface.

at the metal-air interface.

### A.0.5 Why TE modes of SPP cannot exist

Using (A.9), we can write, for $z > 0$

$$E_y(z) = A_2 e^{iKx} e^{-k_2 z} \tag{A.18a}$$

$$H_x(z) = -iA_2 \left(\frac{1}{\omega\mu_0}\right) k_2 e^{iKx} e^{-k_2 z} \tag{A.18b}$$

$$H_z(z) = A_2 \left(\frac{K}{\omega\mu_0}\right) e^{iKx} e^{-k_2 z} \tag{A.18c}$$

and for $z < 0$

$$E_y(z) = A_1 e^{iKx} e^{k_1 z} \tag{A.19a}$$

$$H_x(z) = iA_1 \left(\frac{1}{\omega\mu_0}\right) k_1 e^{iKx} e^{k_1 z} \tag{A.19b}$$

$$H_z(z) = A_1 \left(\frac{K}{\omega\mu_0}\right) e^{iKx} e^{k_1 z} \tag{A.19c}$$

The continuity of $E_y$ at the interface ($z = 0$) requires that $A_1 = A_2$. Continuity of $H_x$ at the interface requires that $A_1(k_1 + k_2) = 0$. Since both $k_1$ and $k_2$ have to be positive in order to have evanescently decaying waves in the perpendicular direction to the interfaces in both the media, this condition is satisfied only when $A_1 = 0$ and in turn, $A_2 = 0$. That means, TE modes (s polarized) of Surface Plasmon Polaritons do not exist at all. This explains the experimental results we obtained.